

Subjective Annotation for a Frame Interpolation Benchmark using Artifact Amplification

Hui Men¹ · Vlad Hosu¹ · Hanhe Lin¹ · Andrés Bruhn² · Dietmar Saupe¹

the date of receipt and acceptance should be inserted later

Abstract Current benchmarks for optical flow algorithms evaluate the estimation either directly by comparing the predicted flow fields with the ground truth or indirectly by using the predicted flow fields for frame interpolation and then comparing the interpolated frames with the actual frames. In the latter case, objective quality measures such as the mean squared error are typically employed. However, it is well known that for image quality assessment, the actual quality experienced by the user cannot be fully deduced from such simple measures. Hence, we conducted a subjective quality assessment crowdsourcing study for the interpolated frames provided by one of the optical flow benchmarks, the Middlebury benchmark. It contains interpolated frames from 155 methods applied to each of 8 contents. For this purpose, we collected forced choice paired comparisons between interpolated images and corresponding ground truth. To increase the sensitivity of observers when judging minute difference in paired comparisons we introduced a new method to the field of full-reference quality assessment, called artifact amplification. From the crowdsourcing data (5887 participants, 3720 comparisons of 50 votes each) we reconstructed absolute quality scale values according to Thurstone’s model. As a result, we obtained a re-ranking of the 155 participating algorithms w.r.t. the visual quality of the interpolated frames. This re-ranking not only shows the necessity of visual quality assessment as another evaluation metric for optical flow and frame interpolation benchmarks, the results also provide

the ground truth for designing novel image quality assessment (IQA) methods dedicated to perceptual quality of interpolated images. As a first step, we proposed such a new full-reference method, called WAE-IQA. By weighing the local differences between an interpolated image and its ground truth WAE-IQA performed slightly better than the currently best FR-IQA approach from the literature.

Keywords Visual Quality Assessment · Frame Interpolation · Artifact Amplification · Weighted Error

1 Introduction

As one of the basic video processing techniques, frame interpolation, namely computing interpolated in-between images in image sequences, is a necessary step in numerous applications such as temporal up-sampling for generating slow motion videos [14], nonlinear video re-timing in special effects movie editing [20], and frame rate conversion between broadcast standards [22]. One of the main concepts in frame interpolation is motion compensation. In this context, required frames are obtained by interpolating the image content along the path of motion. Thereby, the apparent motion in terms of the so-called optical flow can be derived in various ways. Typical approaches for this task include block matching techniques [10], frequency-based approaches [22], variational methods [26] or convolutional neural networks [2, 14].

Since the quality of the interpolated frames heavily depends on the underlying optical flow algorithm, the evaluation of the results is a critical issue. However, currently, there is only one optical flow benchmark that offers the assessment of interpolated frames: the Middlebury benchmark [1]. Regarding the quality of the motion estimation, it considers angular and endpoint errors between the

Funded by the Deutsche Forschungsgemeinschaft (DFG, German Research Foundation) Project-ID 251654672 TRR 161 (Project A05 and B04).

¹ Department of Computer and Information Science, University of Konstanz, Germany. E-mail: {hui.3.men, vlad.hosu, hanhe.lin, dietmar.saupe}@uni-konstanz.de

² Institute for Visualization and Interactive Systems, University of Stuttgart, Germany. E-mail: bruhn@vis.uni-stuttgart.de

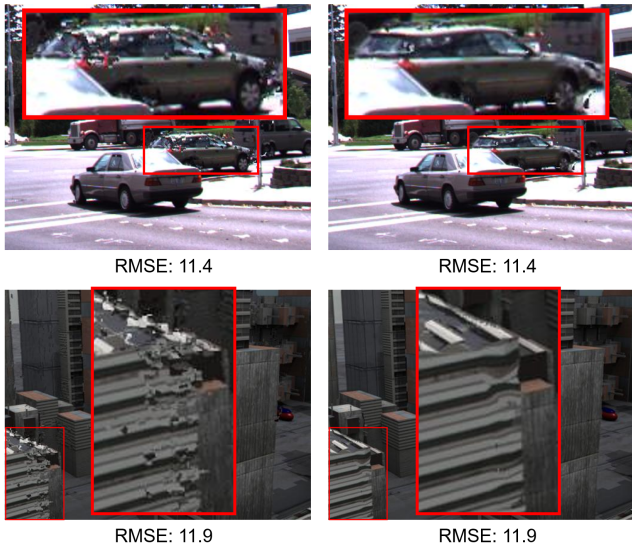


Fig. 1 Two interpolated frames, each with two different methods. RMSE values in each pair are equal, but the visual quality differs in each pair, in particular in the zoomed regions.

estimated flow and the ground truth flow. More importantly, it also offers a direct evaluation of the corresponding motion-compensated interpolation results between frame pairs, which is based on the root mean squared error (RMSE) and the gradient normalized RMSE between the interpolated image and the ground truth image.

In general, the direct evaluation of the frame interpolation results is useful, since the accuracy of the motion estimation is not always directly related to the quality of the motion-compensated frame interpolation. For example, motion errors in low-textured regions are less noticeable in the interpolation result than motion errors in highly-textured regions. However, specifically designed error measures such as the gradient normalized RMSE even revert this relation and penalize interpolation errors in high-textured regions less severely which adapts the error measure to the shortcomings of motion-based frame interpolation techniques instead of trying to assess the frame interpolation quality adequately. Moreover, it is well known that even the standard mean square error can be misleading and may not reliably reflect image quality as perceived by the human visual system (HVS) [36]. This fact also becomes obvious from the Middlebury web-page, where some of the interpolated images have the same RMSE but exhibit obvious differences in image quality (see Fig. 1). Evidently, there is a clear need to improve the assessment of motion-compensated interpolation results. Therefore, we propose to change the quality assessment in such a way that the evaluation of the results takes perceived visual quality assessment into consideration.

Regarding visual quality assessment methods, we take full-reference image quality assessment (FR-IQA) into consideration, since ground truth in-between images are available in the Middlebury benchmark. There are several FR-

IQA methods that consider the HVS, which were designed to estimate image quality degradation due to common artifacts, namely the ones caused by processing such as data compression or by losses in data transmission. However, the artifacts induced by optical flow algorithms lead to interpolated images with different specific distortions (see Fig. 2).



Fig. 2 Specific distortions in interpolated images. Left column: detail of the ground truth images *Backyard* and *Basketball*. Right column: corresponding detail of its interpolated counterparts (with distortions).

In this article we show that seven of the most popular objective FR-IQA methods have rather low correlations with the evaluations made by human observers, regardless of whether the methods are based on the HVS or just on pixel-wise errors such as RMSE; see Table 3 (in Section 7). The VSI [42] method is one of the best FR-IQA methods. When trained and tested on the LIVE database it yields a Spearman rank-order correlation coefficient (SROCC) of 0.952 w.r.t. ground truth consisting of mean opinion scores (MOS) from a controlled lab study [29]. However, even VSI only gave a SROCC of 0.6577 w.r.t. MOS reconstructed from paired comparisons when applied to the interpolated images by optical flow algorithms. This demonstrates that current FR-IQA methods are not able to cope with the specific distortion types that arise in interpolated frames produced by optical flow algorithms. Therefore, a new FR-IQA method specifically designed for such images is needed. However, before the research in such FR-IQA methods can proceed, ground truth data, namely subjective quality scores of such images need to be collected, a first set of which is provided by our study.

Regarding the subjective quality evaluation, lab-studies are well established due to their reliability. In particular, the experimental environment and the evaluation process can be controlled. However, it is time consuming and costly, which severely limits the number of images to be assessed. In contrast, crowdsourcing studies can be less expensive. Moreover, the reliability of crowdsourcing has been proven to be acceptable, if the setup is appropriate and the crowd workers are trained [28].

In our preliminary work, [21], with the help of crowdsourcing, we have implemented paired comparisons to collect subjective quality scores of the interpolated images in the Middlebury benchmark, denoted as *StudyMB 1.0*. However, the limitation of *StudyMB 1.0* is that the quality differences between some of the images are hardly visible. Even though in the instructions we had highlighted the main degraded parts according to our visual observation, still some of the image pairs could not be well judged by the subjects. For instance, both of the images shown in Fig. 3, which were displayed as a pair in *StudyMB 1.0*, were assigned the same quality score, although the quality differences between them become obvious when inspected in detail.

Thus, we improved the design of the subjective study in the following two ways. (1) Artifact zooming: We help users identify the degradation by providing zoomed image portions that contain the most noticeable artifacts. (2) Artifact amplification: We increase the local contrast of the images without significantly changing the average color properties of the images in the changed areas.

In this paper, we implemented this improved paired comparisons of interpolated images given by optical flow algorithms in the Middlebury interpolation benchmark and re-ranked them accordingly (denoted as *StudyMB 2.0*). Comparing the old ranking according to RMSE in the Middlebury benchmark and the re-ranking according to our improved subjective study then allows us to judge the suitability of existing quality metrics.

The outcome of our study is clear. It demonstrates that current FR-IQA methods are not suitable for assessing the perceived visual quality of interpolated frames that have been created by using optical flow algorithms. Therefore, using the collected subjective scores as ground truth, we propose a novel FR-IQA method. It is based on a weighted absolute error (WAE) which locally assigns different weights to absolute errors between the interpolated image and its ground truth. The average result of the leave-one-out (LOO) cross validation shows that WAE-IQA offers a slightly better performance for the interpolated Middlebury images than the currently best FR-IQA method from the literature.

Summarizing, compared to [21], the contribution of the current journal paper is threefold:

- We provide better subjective quality scores via artifact amplification and zooming, which serve as a basis for the development and evaluation of new FR-IQA methods.
- Based on the new scores, we reveal the poor performance of existing FR-IQA methods when predicting the quality of motion compensated frame interpolation.
- We further propose a weighted error based FR-IQA method, which is specifically designed for the frame interpolation with motion compensation.

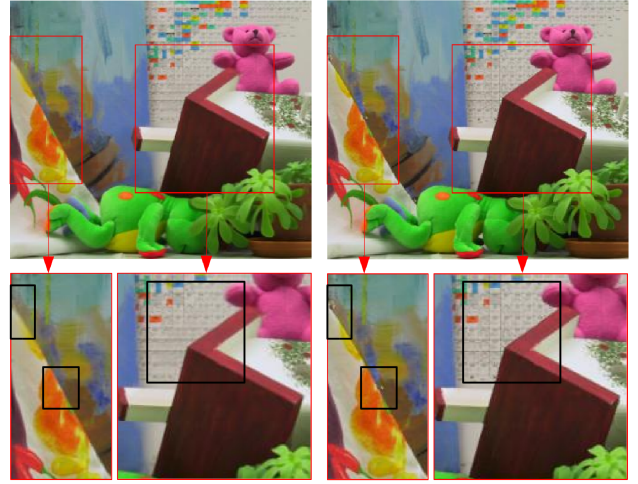


Fig. 3 A pair of images that obtained the same average score in *StudyMB 1.0*. However, quality differences exist, especially in the zoom-in parts (see the portions in black rectangles).

2 Related Work

As the recent literature on frame interpolation shows, there is mainly one benchmark that is considered for evaluating the performance of frame interpolation methods: the Middlebury benchmark. Originally designed for the evaluation of optical flow algorithms, this benchmark also offers an evaluation of motion-based frame interpolation results based on the calculated optical flow. To this end, it compares the interpolated frames with the ground truth in-between images that have been obtained by recording or rendering the original image sequence with a higher frame rate. Hence, despite of its original focus on evaluating optical flow methods, in the last few years this benchmark has become the de facto standard for the evaluation and comparison of frame interpolation algorithms; see e.g. [22, 23, 26].

Apart from the Middlebury benchmark, there are also two other datasets that are, however, less frequently considered for evaluation. While some interpolation algorithms like [9, 17] use the UCF 101 dataset [30] for training

and testing, others like [8, 40] considered the videos from [33, 34].

Regarding the assessment of the interpolation quality, both the Middlebury benchmark and the other data sets rely on standard metrics, such as MSE, PSNR, or SSIM to measure the differences between the interpolated result and the ground truth in-between image. However, to the best of our knowledge, there have been no attempts so far to analyze how useful these metrics actually are to measure the quality of motion-compensated frame interpolation.

Regarding the amplification of artifacts we applied pixel value range expansion. This method was so far only adopted in reverse tone mapping operators (rTOMs), aiming to give low dynamic range images (LDR) the appearance of a higher dynamic range (HDR) without annoying artifacts [35]. The general technique of rTOM first identifies the brightest areas of the image, yielding a certain kind of expansion map. Those bright areas are then expanded to a significant extent using different dynamic range expansion functions, whereas the rest of the pixels of the image are kept unchanged or only slightly modified [19]. To the best of our knowledge, such idea of amplifying the pixel value range for increasing the error visibility was not adopted in any subjective image quality assessment study so far.

3 Prior Knowledge

3.1 Subjective Study

Absolute Category Rating (ACR) is a type of subjective testing where the test items are presented one at a time and are rated independently on one of five possible ordinal scales, i.e., Bad-1, Poor-2, Fair-3, Good-4, and Excellent-5 [13].

ACR is easy and fast to implement, however, it has several drawbacks [4]. Participants may be confused when the categories of the rating scale have not been explained sufficiently well. They may also have different interpretations of the ACR scale, in particular in crowdsourcing experiments because of the wide range of cultural backgrounds and perceptual experiences of the crowd workers.

Moreover, the perceptual distances between two consecutive scale values, e.g., between 1 and 2, should ideally be the same. However, in practice this can hardly be achieved [12]. Also it is not easy to detect when a participant intentionally or carelessly gives false ratings. Alternatively, *paired comparisons* (PC) can solve some of the problems of ACR. In a PC test, items to be evaluated are presented as pairs. In a forced choice setting, one of the items must be chosen as the preferred one. The main advantage of this strategy is that it is highly discriminatory, which is very relevant when test items have nearly the same quality.

However, when implemented naively, comparing N items would require $\binom{N}{2}$ comparisons, too many to be prac-

tical, when N is on the order of 100, for example. In our case, for each of the 8 sequences, we would have to compare $N = 155$ images, giving a total of 95,480 pairs.

A practical solution to this problem is to resort to the concept of randomly paired comparisons that is based on randomly choosing a fraction of all possible paired comparisons. This strategy is not only more efficient, it also has been proven to be as reliable as full comparisons [38]. After obtaining results from these comparisons, subjective scores have to be reconstructed. This can be done based on Thurstone's model [18, 31] or the Bradley-Terry model [3].

3.2 Thurstone's Model

Thurstone's model provides the basis for a psychometric method for assigning scale values to options on a 1-D continuum from paired comparisons data. It assumes that an option's quality is a Gaussian random variable, thereby accommodating differing opinions about the quality of an option. Then each option's latent quality score is revealed by the mean of the corresponding Gaussian.

The result of a paired comparison experiment is a square count matrix C denoting the number of times that each option was preferred over any other option. More specifically, for n comparisons of option A_i with option A_j , $C_{i,j}$ gives the number of times A_i was preferred over A_j . Similarly, $C_{j,i}$ in the count matrix denotes the number of times that A_j was preferred over A_i , and we have $C_{i,j} + C_{j,i} = n$.

According to Thurstone's Case V, subjective qualities about two options A and B are modelled as uncorrelated Gaussian random variables A and B with mean opinions μ_A , μ_B and variances σ_A^2 , σ_B^2 , respectively. When individuals decide which of the two options is better, they draw realizations from their quality distributions, and then choose the option with higher quality. More specifically, they choose option A over option B if their sample from the random variable $A - B$ (with mean $\mu_{AB} = \mu_A - \mu_B$ and variance $\sigma_{AB}^2 = \sigma_A^2 + \sigma_B^2$) is greater than 0. Therefore, the probability of a subject to prefer option A over B is:

$$P(A > B) = P(A - B > 0) = \Phi\left(\frac{\mu_{AB}}{\sigma_{AB}}\right), \quad (1)$$

where $\Phi(\cdot)$ is the standard normal cumulative distribution function (CDF).

Thurstone proposed to estimate $P(A > B)$ by the empirical proportion of people preferring A over B, which can be derived from the count matrix C as:

$$P(A > B) \approx \frac{C_{A,B}}{C_{A,B} + C_{B,A}}. \quad (2)$$

The estimated quality difference $\hat{\mu}_{AB}$ can be derived from inverting Eq. 1, giving:

$$\hat{\mu}_{AB} = \sigma_{AB} \Phi^{-1} \left(\frac{C_{A,B}}{C_{A,B} + C_{B,A}} \right) \quad (3)$$

known as Thurstone’s Law of Comparative Judgment, where $\Phi^{-1}(\cdot)$ is the inverse standard normal CDF, or z-score. Least-squares fitting or maximum likelihood estimation (MLE) can be then applied to estimate the scale values μ_A for all involved stimuli A . For more details we refer to [32].

4 Subjective Quality Assessment: StudyMB 2.0

4.1 Data and Study Design

In order to re-rank the methods in the Middlebury benchmark, we implemented paired comparisons based on Thurstone’s model with least-squares estimation to obtain subjective judgments of the image qualities. In the benchmark, there are 8 sets of 155 interpolated images each, most of which had been generated by optical flow methods.¹ To run a complete set of possible comparisons would require collecting ratings for $8 \times 155 \times 154/2$ pairs, which is too many for practical purposes. However, it is sufficient to compare only a subset of these pairs. Therefore, we randomly sample pairs within each of the 8 sets, such that the 155 images form a random sparse graph with a vertex degree of 6 i.e., each image was to be randomly compared to exactly 6 other images, which resulted in $465 \times 8 = 3720$ pairs of images.

We ran the experiment using the Figure Eight platform [7]. In total there were 47 tasks in the job, each consisting of one page. Each page we showed 10 sequences of 8 pairs of images. In each sequence one pair of images from each of the 8 contents of the benchmark were selected (i.e., 8 pairs of images starting from *Mequon* until *Evergreen*). Payments were initiated for each completed page. For each pair of images to be compared, we collected 50 votes from the crowd workers. In total there are 5887 crowd workers participated in the eight jobs.

In order to increase the sensitivity of the subjective detection of minute differences between two interpolated images, we applied two methods.

- (1) **Artifact amplification.** Interpolated images in the benchmark differ from the ground truth images. The pixel-wise differences w.r.t. the ground truth images were artificially increased for display and judgment.
- (2) **Artifact zooming.** Artifacts due to interpolation based on optical flow tend to be localized in images, for example nearby edges of moving objects. To steer the attention of the crowd workers towards these most heavily

degraded image portions, these regions were displayed also enlarged below the full image above.

The crowdsourcing interface for one comparison as shown in Fig. 4. It contains the zoomed image regions with the most severe distortions for each of the images to be compared and additionally the ground truth image, in full size and with the zoomed portion. In the next two subsections we give the details for these two methods.

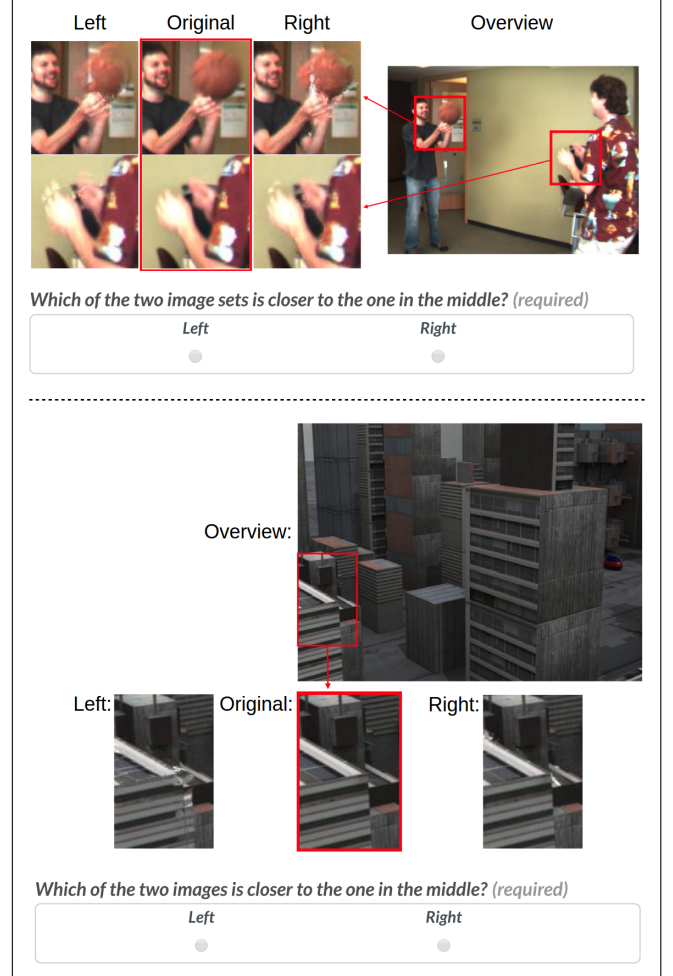


Fig. 4 Interface of the crowdsourcing experiment. The full-sized ground truth image was displayed in the experiment overview section, with the most noticeable degraded parts highlighted. Zoomed portions of the interpolated images were provided as pairs, with the ground truth placed in the middle.

4.1.1 Artifact Amplification by Local RGB Transformation

Since the human visual system is not sensitive enough to reliably detect the quality differences for many of the interpolated images [21], we artificially emphasized the defects by linearly scaling up the differences relative to the ground

¹ When we ran the experiments in March 2019, there were altogether 155 methods in the Middlebury benchmark, including a number of additional, new methods compared to [21]

truth. Following Weber's law [6], given an interpolated image, we basically enlarged the RGB pixel differences for all pixels linearly, following

$$\hat{v}' = v + \alpha(\hat{v} - v),$$

where v is an original RGB (ground truth) component value, and $\alpha \geq 1$ is a fixed amplification factor. For 24 bit color images, the transformed RGB component values should not be outside the range $[0, 255]$, which could be achieved by common clamping. However, clamping is a nonlinear operation which might actually remove differences in artifacts between two interpolated images. Therefore, we propose to reduce the amplification factor α at pixels where the linear RGB transformation would require clamping, to the maximal α without requiring clamping. See Algorithm 1 for the details.

Algorithm 1 Pixel-wise Artifact Amplification

```

1:  $\alpha :=$  default value, e.g., 4 ;
2:  $v := (v_r, v_g, v_b)$ ; {ground truth image pixel}
3:  $\hat{v} := (\hat{v}_r, \hat{v}_g, \hat{v}_b)$ ; {interpolated image pixel}
4: for  $r$  component do
5:   if  $\hat{v}_r - v_r > 0$  then
6:      $\alpha_{max_r} = (255 - v_r) / (\hat{v}_r - v_r)$ ;
7:   else if  $\hat{v}_r - v_r < 0$  then
8:      $\alpha_{max_r} = -v_r / (\hat{v}_r - v_r)$ ;
9:   else
10:     $\alpha_{max_r} = \alpha$ ;
11:   end if
12: end for
13: for  $g, b$  components do
14:   same as above for  $r$  component;
15: end for
16:  $\alpha := \min(\alpha, \alpha_{max_r}, \alpha_{max_g}, \alpha_{max_b})$ ;
17:  $v' := v + \alpha(\hat{v} - v)$ .
```

As shown in Fig. 5, before the pixel value range amplification, it is extremely hard to distinguish the quality differences between the original pair of images. After the amplification the differences become much more obvious and thus easier for participants in our experiment to provide reliable annotations.

4.1.2 Artifact Zooming

In addition to boosting pixel value differences, we also zoomed into the relevant regions that have the most noticeable degradation. Such regions of each set of images were extracted via the following steps (see Fig. 6):

– *Step 1: Gaussian Smoothed Average Error Image*

For the n -th image I_n of 155 interpolated images from the same scene, the absolute error compared to the ground truth image I_0 was first computed, giving an absolute error image $E_n = |I_n - I_0|$.

The mean of all 155 absolute error images is

$$E_{avg} = \frac{1}{155} \sum_{n=1}^{155} |I_n - I_0|.$$

A Gaussian filter (standard deviation of 20) was applied to the average error image E_{avg} , resulting in the Gaussian smoothed average error image, \tilde{E}_{avg} .

– *Step 2: Segmentation*

Using Otsu's method [24], the smoothed average error image \tilde{E}_{avg} was segmented into two or more parts. The most noticeable degraded portions were then extracted by bounding boxes around the segmented parts.

4.2 Quality Assurance and Quality Control

Before the actual paired comparison, there was a training session, in which workers were instructed how to compare the quality of images. Since the visual differences between some images are not that obvious, we explained in the instructions how to compare the image quality; see Fig. 7.

In order to assure the reliability of the crowd workers, the unreliable ones need to be detected and disallowed to continue. This was done by requiring crowd workers to answer test questions. For the test questions we chose image pairs with the ground truth in-between image as one of the images, and the other image of bad quality. Then the expected, correct answer, was obviously given by choosing the ground truth image as the one with a better quality.

Before crowd workers were allowed to start a job, they had to pass a quiz which was composed entirely of test questions. This ensures that only capable crowd workers that proved to be able to work on the subject matter of the job, would be able to enter the job. Crowd workers that failed the quiz were permanently disqualified from working on the job. After passing the quiz, crowd workers were admitted to start the real job. During the job, they had to answer further hidden test questions. Once a crowd worker failed more than 30% of the hidden test questions, he or she was disqualified and removed from the job. Only crowd workers who passed the quiz and showed an accuracy above 70% on the hidden test questions were regarded as reliable.

5 Re-ranking Results

In our study we chose to compare image pairs only within each of the eight sets of 155 images. Using the collected comparative judgments we reconstructed absolute quality scale values for each image using Thurstone's model and the code provided by [32]. However, because we did not have cross-set comparisons available, the range of values reconstructed for each set are independent of each other. We

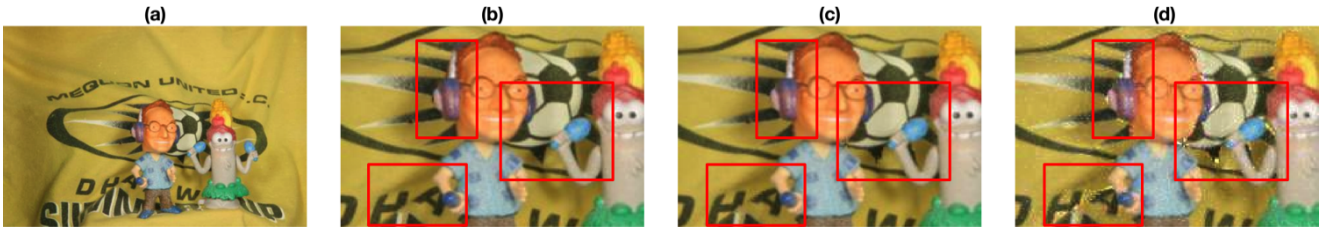


Fig. 5 (a) Full size ground truth image of *Mequon*. (b) Zoomed part of (a). (c) Zoomed part of an interpolated image (original, without artifact amplification). (d) Artifact amplified version of (c). Distortions in (d) are more visible than in (c), especially for the parts in the red rectangles.

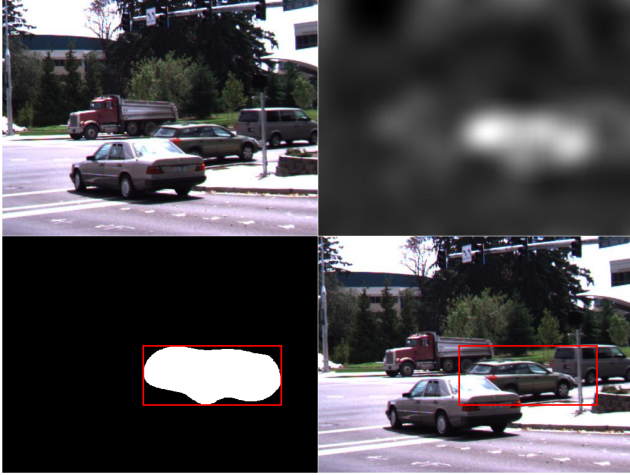


Fig. 6 Extraction of the most noticeable degraded portions of *Dumptruck*. Upper left: average image (of 155 images in total). Upper right: Gaussian smoothed average error image \bar{E}_{avg} . Lower left: segmentation of \bar{E}_{avg} using Otsu's method. Lower right: corresponding bounding box in the original image.

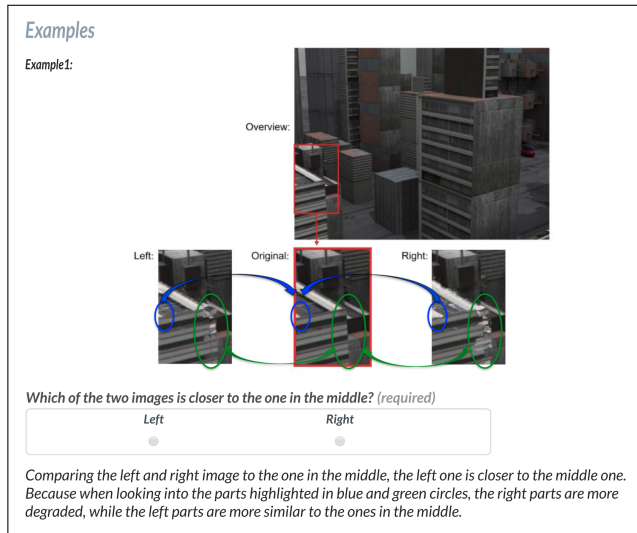


Fig. 7 Instructions of crowdsourcing experiment.

propose a simple procedure to align the reconstructed scales, by introducing virtual anchors. We added two fictitious images as anchors. One of them represents the worst quality among all the images, and the other one is like the ground

truth image, with a quality that is better than that of all the other images.

After reconstruction of the scale values for the 155+2 images in each set, we linearly rescaled the quality scores such that the quality of the virtual worst quality image became 0, and that of the ground truth image became 1. In this way, we rescaled the reconstructed scores to the interval $[0, 1]$. All reconstructed quality values, accompanied by their corresponding rankings, are shown in Table 4 and 5. The differences between the re-ranking (ranked according to subjective study) and their corresponding ranking in the Middlebury benchmark (ranked according to RMSE) are shown in Table 6 and 7.

Each set was scaled and ranked separately. Then the average quality of a method was obtained by taking the mean of the (scaled) quality values of the 8 sets, which resulted in an overall rank. Fig. 8 shows the histogram of the reconstructed quality scores of all the 8 sets of images. Besides, the histogram of the average quality scores of 155 methods is depicted in Fig. 9.

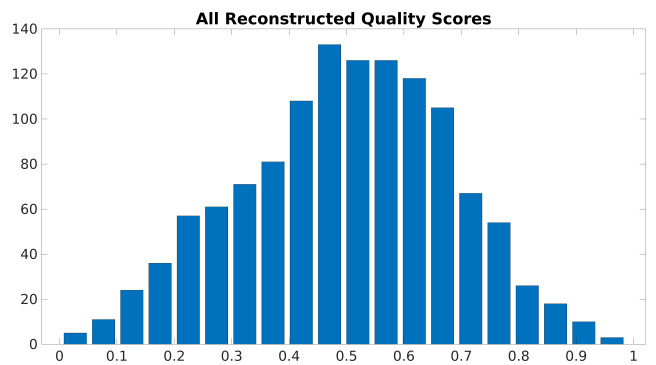


Fig. 8 Histogram of reconstructed quality scores of all the 8 sets of images obtained in StudyMB 2.0.

The best three methods ranked by the subjective study, i.e., CtxSyn [23], CyclicGen [16], and SuperSloMo [14], ranked 2nd, 1st, and 3rd in the Middlebury benchmark, respectively. Overall, as shown in Fig. 10, 49 methods showed (average) rank differences up to 10, and 45 methods gave

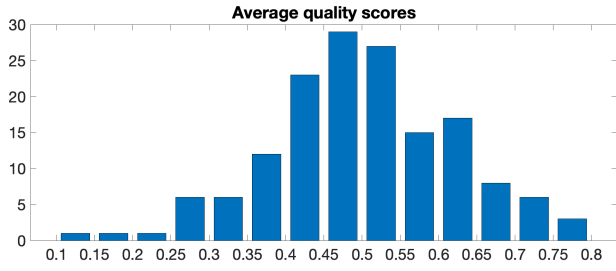


Fig. 9 Histogram of average quality scores over 8 sets obtained in StudyMB 2.0.

(average) differences of more than 30 between their re-rankings and the rankings in the Middlebury benchmark.²

As an overall analysis, Table 1 shows the bootstrapped (after 1000 iterations) SROCC values accompanied by the 95% confidence intervals (CI) between the ranking in the Middlebury benchmark (i.e., ranking according to RMSE) and the re-ranking according to our subjective study. Note that the CI of SROCC was computed by transforming the rank correlation score into an approximate z-score using the Fisher transform [27]. In a nutshell, a CI of probability p is given by $\tanh(\arctan r \pm \Phi^{-1}(p)/\sqrt{n-3})$, where r denotes the estimated SROCC, n is the sampling size, and Φ^{-1} is the inverse of the standard normal CDF. In order to visualize the result, we computed the disagreement level as $1 - \text{SROCC}$ as shown in Fig. 11.

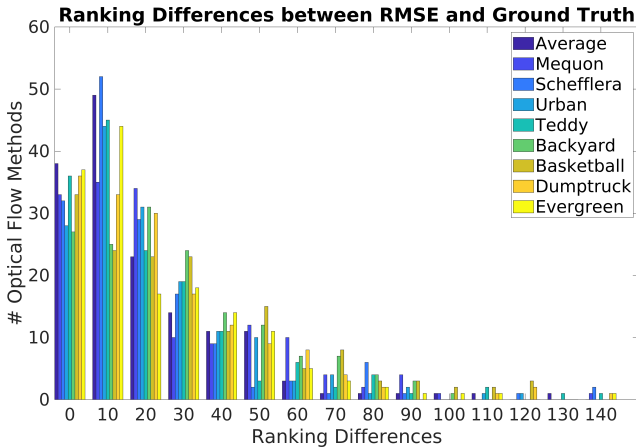


Fig. 10 Ranking differences between RMSE and Ground Truth (by StudyMB 2.0).

6 Comparisons between StudyMB 2.0 and 1.0

As mentioned before, we implemented StudyMB 1.0 in our preliminary work [21]. Similar as StudyMB 2.0, in

² Some methods are specifically tailored for frame interpolation (e.g., SuperSloMo) and some are only tailored for optical flow estimation (e.g., DeepFlow2).

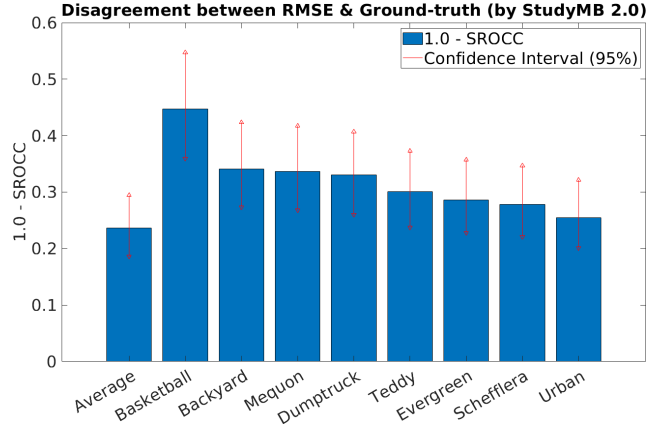


Fig. 11 Disagreement level with 95% confidence interval.

StudyMB 1.0, we also used paired comparisons and crowd-sourcing to collect subjective quality scores of the interpolated images in the Middlebury benchmark. However, there exist a number of differences between these two experiments, leading to differences in the subjective scores obtained.

6.1 Differences in Data

In StudyMB 1.0, we evaluated the interpolation performances of 141 optical flow methods. 14 more methods were added in StudyMB 2.0, resulting in 155 optical flow methods. Note that for later comparisons between these two experiments, we ignored those 14 more methods in StudyMB 2.0 to make them comparable.

Regarding the scale of the subjective study, in StudyMB 2.0, we collected 20 more votes from each crowd worker than that in StudyMB 1.0 (i.e., we collected 30 votes in StudyMB 1.0 and 50 votes in StudyMB 2.0). This leads to an increase of the precision of the subjective study.

6.2 Differences in Study Design

The first difference regarding study design is that, instead of launching eight separate jobs (in StudyMB 1.0), each of which consists of the same contents, we mixed all the eight sets as one job in StudyMB 2.0. This avoided the phenomenon of semantic satiation [5, 25] which can occur not only in text but also in images.

The other difference is that in the instructions of StudyMB 2.0, we did not only highlight degraded parts as in StudyMB 1.0, but we also amplified the pixel value range of the interpolated images for increasing the visibility of the quality differences and zoomed the most noticeable parts, in order to draw attention to the regions of interest and make it easier for participants to perform their task.

Table 1 Correlations between RMSE and Ground Truth (by StudyMB 2.0) after 1000 Iterations.

RMSE	Average	Mequon	Schefflera	Urban	Teddy	Backyard	Basketball	Dumptruck	Evergreen
SROCC	0.7637	0.6630	0.7217	0.7455	0.6990	0.6590	0.5529	0.6696	0.7143
CI (95%)	[0.7058, 0.8136]	[0.5824, 0.7320]	[0.6531, 0.7787]	[0.6786, 0.7988]	[0.6271, 0.7623]	[0.5763, 0.7266]	[0.4527, 0.6402]	[0.5936, 0.7398]	[0.6426, 0.7719]

6.2.1 Sensitivity to Quality Differences

As described in Equation 2, the probability $P(A > B)$ in the count matrix C denotes the empirical proportion of people preferring A over B . Thus, $P = 0.5$ illustrates that options A and B got exactly the same number of votes in the subjective study (i.e., A and B are of the same quality), whereas $P = 0$ or $P = 1$ depicts the fact that either A or B obtained all the votes whereas the other one got no vote (i.e., A or B is much better than the other one). Therefore, the distribution of the probabilities in the count matrices can properly reveal the sensitivity to quality differences of the subjective study. To this end, we computed the cumulative distribution function (CDF) of the aggregated probabilities in all the count matrices (of all the eight sets) for both of the two experiments, and fitted their CDFs to probability density function (PDF). As shown in Fig. 12, the PDF of StudyMB 1.0 approaches a normal distribution with a peak at probability 0.5, which illustrates that for most of the image pairs in the experiment, their quality differences are hardly distinguishable. The PDF of StudyMB 2.0 appears almost complementary to that of StudyMB 1.0, having the form of a Beta distribution ($\alpha = \beta = 0.5$, approximately), indicating that for most of the image pairs in the experiment, their quality differences are obvious. Comparing the PDFs between these two experiments shows that the study design of StudyMB 2.0 leads to a much higher sensitivity to image quality differences for the subjects than that of StudyMB 1.0.

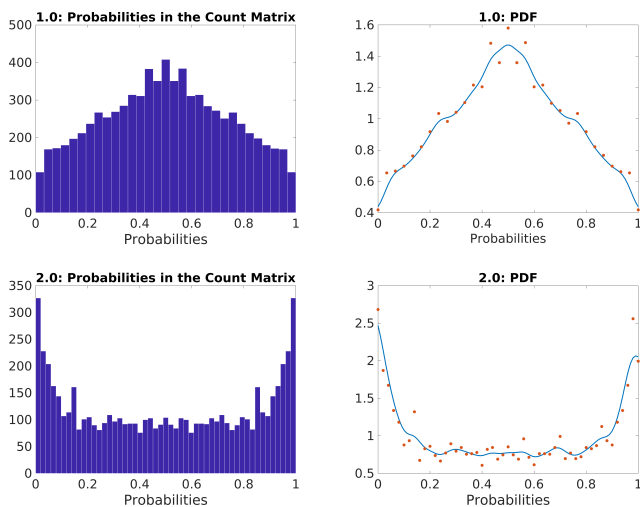


Fig. 12 Upper: Histogram and PDF of aggregated probabilities of all the eight count matrices of StudyMB 1.0 (denoted as 1.0 in the figure). Lower: Histogram and PDF of aggregated probabilities of all the eight count matrices of StudyMB 2.0 (denoted as 2.0 in the figure).

6.2.2 Scale of Quality Scores

As described before, subjective qualities about two options A and B are modelled as uncorrelated Gaussian random variables A and B with means μ_A, μ_B and variances σ_A^2, σ_B^2 , respectively. According to Thurstone’s Case V, all options have equal variance and zero correlations, which is commonly approached by assuming $\sigma_A^2 = \sigma_B^2 = 1$. Conversely, for each reconstructed MOS, its corresponding Gaussian distribution can be plotted using Thurstone’s Case V model. As shown in Fig. 13, 10 out of 141 Gaussian distributions correspond to their respective MOS were sorted from the worst to the best. It is obvious that the spreads of the Gaussian distributions in StudyMB 2.0 are much wider than the ones in StudyMB 1.0, which indicates that the subjective scores obtained in StudyMB 2.0 are better scaled than those in StudyMB 1.0.

6.3 Differences in Subjective Scores

The differences in data and study design between StudyMB 1.0 and StudyMB 2.0 lead to the differences of subjective scores obtained for the interpolated images. In this regard, we investigated the correlations of MOS and re-ranking results between these two experiments.

6.3.1 MOS Correlations

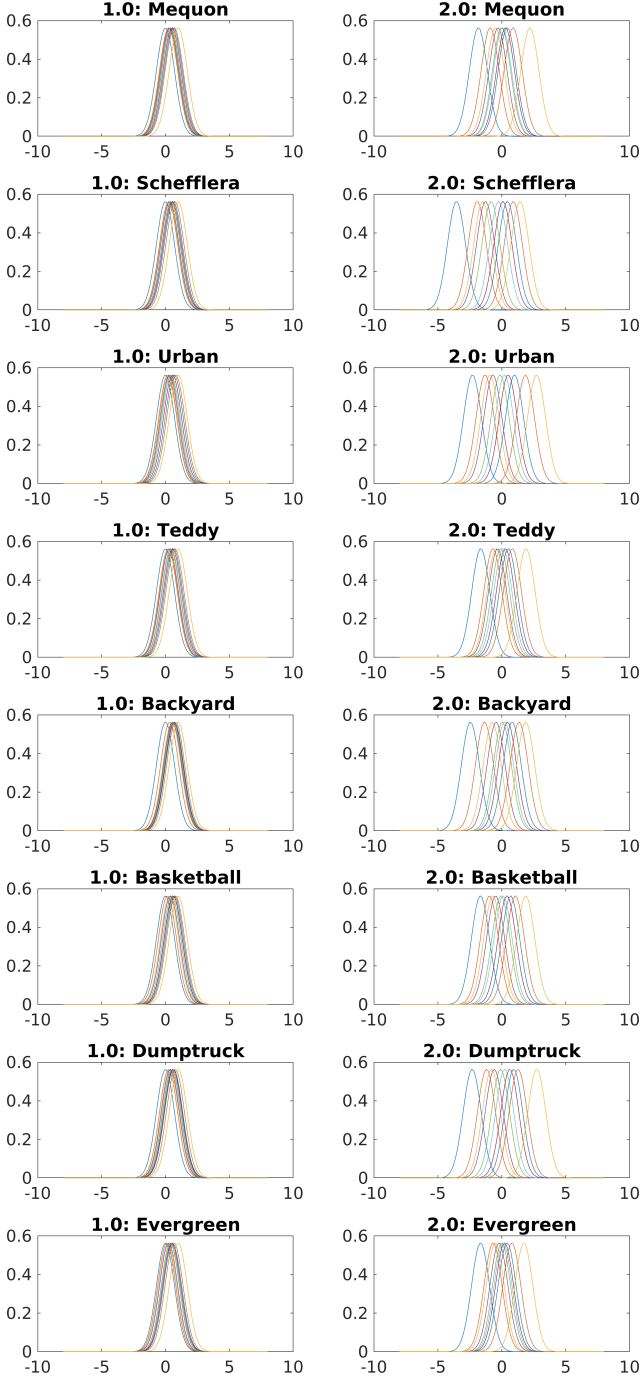
We computed Pearson’s linear correlation coefficient (PLCC), SROCC, and Kendall’s rank-order correlation coefficient (KROCC) between the subjective scores obtained in StudyMB 1.0 and 2.0. As shown in Table 2, the aforementioned three correlations between these two experiments are 0.65 (PLCC), 0.56 (SROCC) and 0.41 (KROCC) on average, which indicates an obvious difference of the subjective quality scores obtained for the same images.

6.3.2 Re-ranking Differences

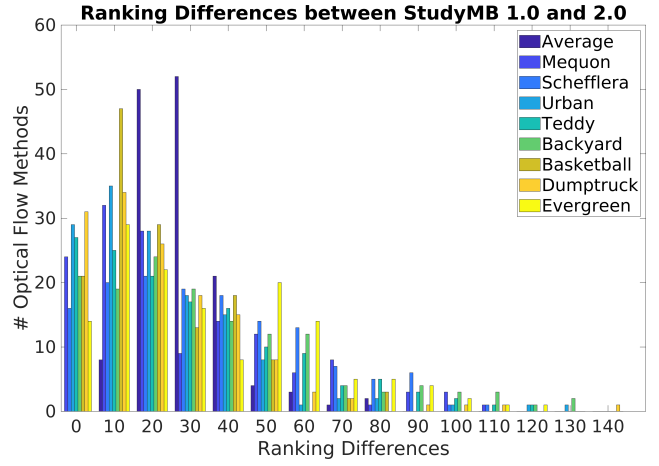
Fig. 14 shows the differences of the re-rankings of 141 optical flow methods between StudyMB 1.0 and 2.0. It can be seen that, on average, there are 8 methods whose re-rankings differ up to 20 places, and 50 methods differ up to 30 places. There are 52 methods having re-ranking differences up to 40 places, and 21 methods showing differences up to 50 places. For the remaining 10 methods, their re-rankings differ more

Table 2 Correlations of Reconstructed MOS between StudyMB 1.0 and 2.0

	Average	Mequon	Schefflera	Urban	Teddy	Backyard	Basketball	Dumptruck	Evergreen
PLCC	0.6479	0.7112	0.5119	0.7343	0.6299	0.4576	0.8054	0.7397	0.5934
SROCC	0.5630	0.5687	0.4381	0.6989	0.5289	0.3580	0.7783	0.7076	0.4253
KROCC	0.4095	0.4134	0.2989	0.5341	0.3582	0.2564	0.5788	0.5418	0.2940

**Fig. 13** Corresponding Gaussian of 10 Methods (sorted ascend: 1, 15, 30, 45, 70, 85, 100, 115, 130, 141) in Study MB 1.0 (left column) and StudyMB 2.0 (right column).

than 50 places. Overall, the re-ranking differences further illustrate that there exist large differences of the quality scores obtained for the same interpolated images between these two experiments.

**Fig. 14** Re-ranking Differences between StudyMB 1.0 and 2.0.

In summary, the main difference between StudyMB 1.0 and 2.0 is that we adopted artifact amplification as well as artifact zooming in StudyMB 2.0, which increased the sensitivity of the subjective study to a large extent. This gives rise to more precise and better scaled subjective quality scores of the interpolated images than the ones obtained in StudyMB 1.0.

7 Weighted Absolute Error as FR-IQA

As described in Section 5, the re-ranking result of our subjective study shows that RMSE cannot reveal the perceptual quality of interpolated frames well. In fact, besides RMSE, most of the current FR-IQA methods cannot cope with the specific distortions that arise in interpolated frames produced by optical flow algorithms. As shown in Table 3, seven of the most popular objective FR-IQA methods, SSIM [36], MS-SSIM [37], MAD [15], FSIM [43], GMSD [39], and VSI [42], gave low correlations with the subjective judgements.

For example, VSI, one of the best FR-IQA methods based on saliency, yielded an SROCC of 0.952 when trained and tested on the LIVE database. However, when we applied the same method to the interpolated images by optical

Table 3 SROCC of Rankings between FR-IQA and Our Subjective Study

FR-IQA	Average	Mequon	Schefflera	Urban	Teddy	Backyard	Basketball	Dumptruck	Evergreen
RMSE	0.6818	0.6681	0.7240	0.7486	0.7035	0.6607	0.5570	0.6752	0.7169
SSIM	0.6701	0.6518	0.7567	0.5895	0.7110	0.6521	0.6691	0.6359	0.6945
MS-SSIM	0.6640	0.6679	0.7676	0.6012	0.7037	0.5701	0.6711	0.6300	0.7003
MAD	0.6212	0.4965	0.6848	0.7013	0.6075	0.6060	0.5590	0.6655	0.6489
FSIM	0.6602	0.6724	0.7274	0.6559	0.6923	0.6120	0.5783	0.6589	0.6841
GMSD	0.6628	0.6210	0.7737	0.6908	0.7059	0.6132	0.5849	0.6257	0.6872
VSI	0.6577	0.6464	0.6194	0.6705	0.7272	0.6261	0.6193	0.6716	0.6810
WAE-IQA	0.6857	0.6656	0.7330	0.7366	0.7139	0.6751	0.5634	0.6772	0.7207

flow algorithms, VSI gave an SROCC of only 0.6577. This is likely due to two reasons:

- The artifacts induced by optical flow algorithms lead to interpolated images that exhibit different, task-specific distortions that are not sufficiently taken into account in the IQA method.
- Saliency based methods like VSI focus on the most salient image regions. However, these may be just those that are not the most severely distorted parts, as shown in Fig. 15b and c.

Furthermore, we extracted the saliency map for the same image using GBVS [11], one of the most widely used saliency detection methods. It can be seen from Fig. 15d that the resulting saliency map differs from the smoothed average error image to a large extent as well.

The other FR-IQA methods mainly rely on a global difference between the distorted image and its ground truth. Let us consider for example SSIM, MAD, FSIM, and GMSD. SSIM and MAD mainly compare the similarity of luminance and contrast between the distorted image and the ground truth. The other two, GSIM and GMSD, are based on the similarity of gradient magnitude. As shown in Fig. 16, the main regions of the errors extracted by these four methods are to some extent similar and consistent with the most noticeable portion as shown in Fig. 6. However, they still could not estimate the perceptual quality of motion-compensated interpolated images well (giving an average SROCC of 0.6701, 0.6212, 0.6602 and 0.6628, respectively). This may be caused by localized distortions, while FR-IQA methods typically make comparisons globally.

To overcome this problem, we propose a method based on weighted absolute error (WAE-IQA). It computes the differences between an interpolated image and its ground truth for each pixel. Only pixels with a sufficiently large interpolation error are fully weighted and pixels with small errors are discounted. In addition a mild nonlinear scaling allows to shape weighted average error for better performance.

The proposed method WAE proceeds as follows (see Fig. 17, 18, and 19).

- Images are converted from RGB to 8-bit grayscale, giving an interpolated grayscale image \hat{I} and the corresponding grayscale ground truth image I .

- The pixelwise absolute errors of \hat{I} are computed and normalized to 1, which gives the normalized absolute error image I' :

$$I' = \frac{1}{255} |\hat{I} - I|.$$

- For normalized absolute errors $x \in [0, 1]$ we define a weight $w(x) \in [0, 1]$ by the logistic function

$$w(x) = \frac{1}{1 + e^{-s(x-t)}},$$

where the slope $s \in [0, \infty)$ and the shift $t \in [0, 1]$ are parameters to be chosen.

- Normalized absolute errors $x \in [0, 1]$ also nonlinearly scaled using a polynomial of degree 3,

$$f(x) = a_1x + a_2x^2 + a_3x^3,$$

where $a_1, a_2, a_3 \in [0, \infty)$ are parameters to be chosen.

- The weighted absolute error is

$$WAE = \frac{\sum_{\text{pixel errors } x} w(x)f(x)}{\sum_{\text{pixel errors } x} w(x)}. \quad (4)$$

We selected the parameters s, t, a_1, a_2, a_3 optimally in terms of SROCC on the training sets in an 8-fold leave-one-out (LOO) cross-validation. We made use of the 155×8 interpolated images in the Middlebury benchmark together with their MOS obtained in our subjective study. For each LOO cross-validation, we used 7 sets for training, and the other set as the test set.

The SROCC results on the test set for each cross-validation is shown in Table 3. On average, WAE-IQA performed slightly better than RMSE. WAE-IQA performed best among all tested FR-IQA methods on three out of eight sets.

8 Conclusion and Future Work

We have adopted a well designed visual quality assessment to the Middlebury benchmark for frame interpolation based mostly on optical flow methods. Using artifact amplification, the sensitivity of our subjective study was increased significantly. Our study confirms that only using

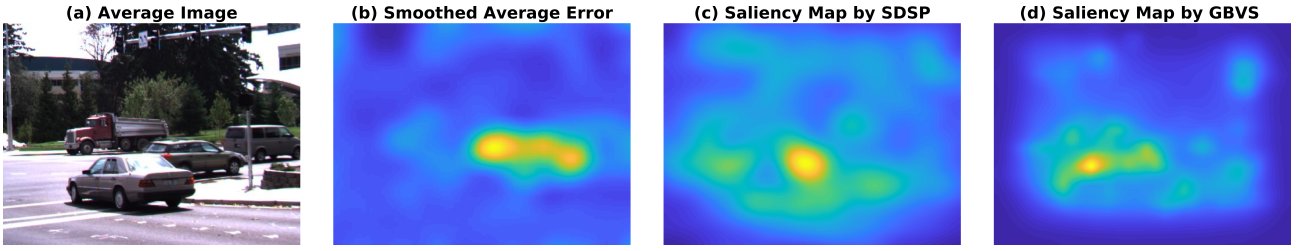


Fig. 15 (a) Average image over 155 interpolated images of *Dumptruck*. (b) Gaussian smoothed average error image (obtained by first taking the average error image over 155 images and then smoothed), which depicts the most degraded parts of image (a) compared to its ground truth. (c) Saliency map of (a) extracted using SDSP [41], the method adopted by VSI. (d) Saliency map of (a) extracted by GBVS.

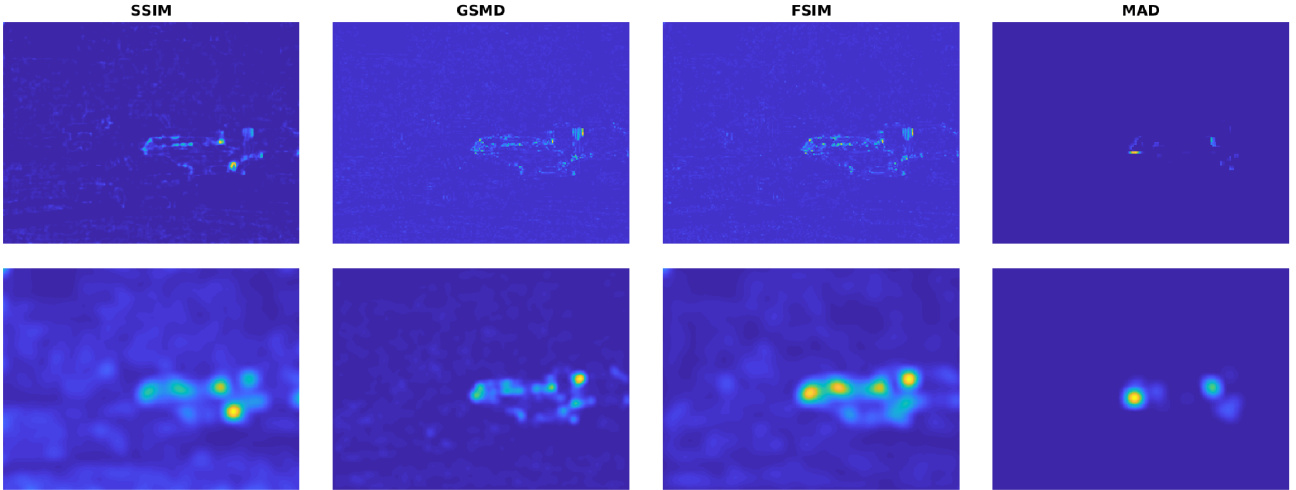


Fig. 16 Visualization of SSIM, GMSD, FSIM, MAD when computing the image quality between the average interpolated image (denoted as *distorted image*) and its ground truth of *Dumptruck*. **Upper row, first three:** distortion maps of SSIM, GMSD and FSI. The brighter the parts are, the more the distorted image differs from its ground truth. **Upper row, the last:** the estimation of the visibility of artifacts in the distorted image given by MAD. Brighter parts denote the higher visibility of the artifacts. **Lower row:** Gaussian smoothed image (of Kernel 10) of its upper corresponding image.

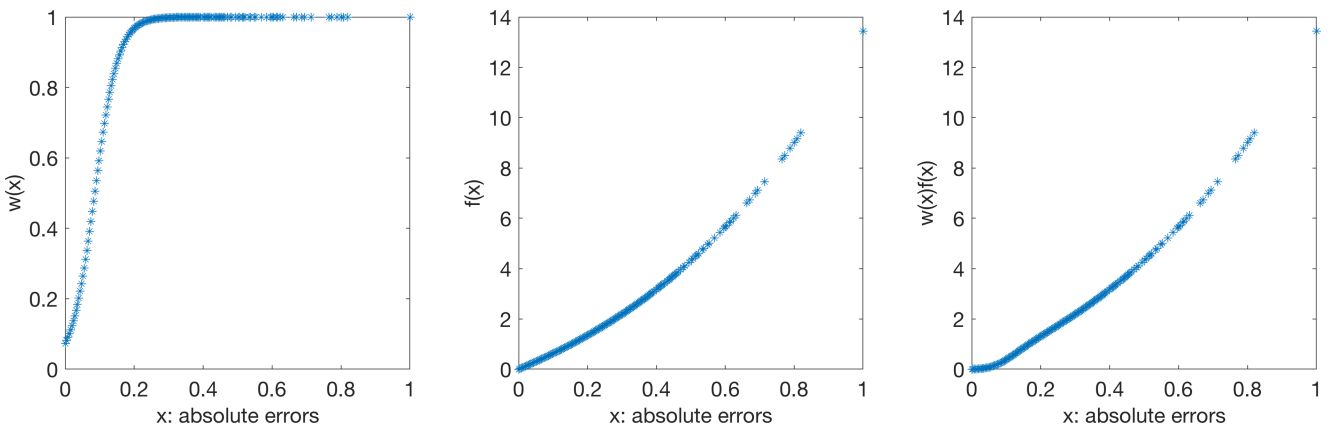


Fig. 17 Related functions in WAE-IQA of *Dumptruck* with parameters $a_1 = 5.8976, a_2 = 3.4039, a_3 = 4.1325, s = 29.6840, t = 0.0855$. Left: logistic weight function $w(x) = 1/(1 + e^{-s(x-t)})$. Middle: Polynomial function of absolute error $f(x) = a_1x + a_2x^2 + a_3x^3$. Right: Weighted absolute error function $w(x)f(x)$.

RMSE as an evaluation metric for image interpolation performance is not representative of subjective visual quality. Also current FR-IQA methods do not provide satisfying results on those interpolated images. This is due to the fact

that such images, especially the ones generated by optical flow algorithms have specific distortions that are quite different from artifacts commonly addressed by conventional IQA methods. Hence, we proposed a novel FR-IQA

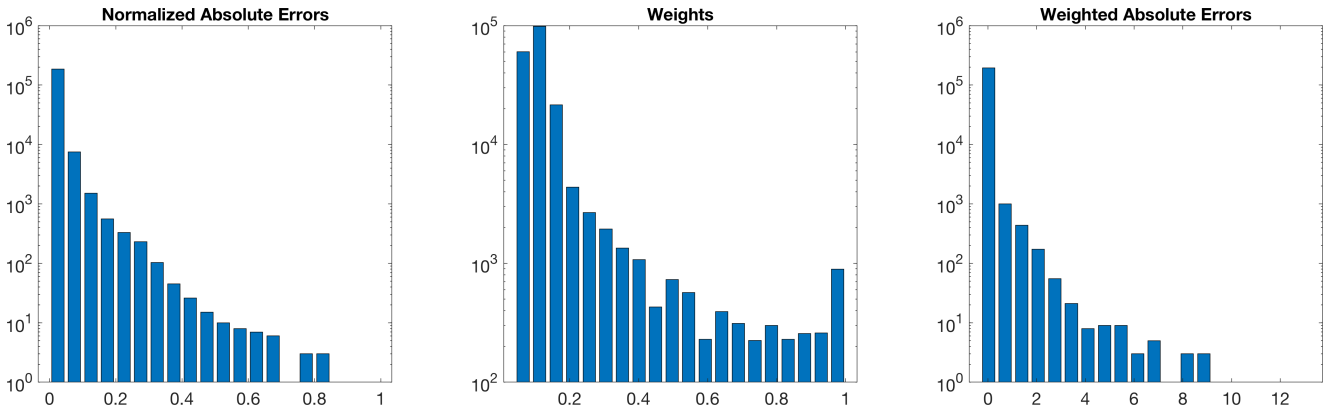


Fig. 18 Histogram of related values in WAE-IQA of *Dumptruck* with parameters $a_1 = 5.8976, a_2 = 3.4039, a_3 = 4.1325, s = 29.6840, t = 0.0855$.

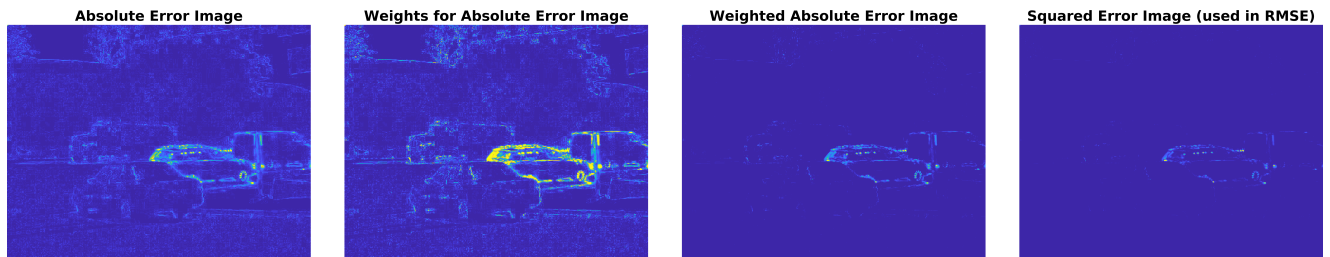


Fig. 19 Visualization of WAE for *Dumptruck* with parameters $a_1 = 5.8976, a_2 = 3.4039, a_3 = 4.1325, s = 29.6840, t = 0.0855$ and squared errors used in RMSE.

method based on a weighted absolute error (WAE-IQA). While this approach outperformed the best FR-IQA method from the literature, the absolute ranking performance only improved slightly. This illustrates that the quality assessment for motion-compensated frame interpolation is a difficult task and there is still plenty of room for improvement.

In the future, we plan to make use of flow fields as side information to further improve the performance of evaluating the perceptual quality of motion-compensated interpolated images. Besides, in order to deal with the specific artifacts caused by motions in such images, we will investigate adopting video saliency detection methods as well as video quality assessment methods based on spatio-temporal information on such images. Furthermore, we will investigate adopting artifact amplification to I/VQA methods in order to improve their performances universally.

Conflict of interest

The authors declare that they have no conflict of interest.

References

1. Baker, S., Scharstein, D., Lewis, J., Roth, S., Black, M.J., Szeliski, R.: A database and evaluation methodology for optical flow. *International Journal of Computer Vision (IJCV)* **92**(1), 1–31 (2011)
2. Bao, W., Lai, W.S., Zhang, X., Gao, Z., Yang, M.H.: MEMC-Net: Motion estimation and motion compensation driven neural network for video interpolation and enhancement. *arXiv e-prints arXiv:1810.08768* (2018)
3. Bradley, R.A., Terry, M.E.: Rank analysis of incomplete block designs: I. the method of paired comparisons. *Biometrika* **39**(3/4), 324–345 (1952)
4. Chen, K.T., Wu, C.C., Chang, Y.C., Lei, C.L.: A crowd-sourceable QoE evaluation framework for multimedia content. In: *ACM International Conference on Multimedia (MM)*, pp. 491–500 (2009)
5. Das, J.P.: *Verbal conditioning and behaviour*. Elsevier (2014)
6. Fechner, G.T., Howes, D.H., Boring, E.G.: *Elements of psychophysics*, vol. 1 (1996)
7. Figure Eight: Figure Eight — The Essential High-Quality Data Annotation Platform (2007). URL <https://www.figure-eight.com/>
8. Ghutke, R.C., Naveen, C., Satpute, V.R.: A novel approach for video frame interpolation using cubic motion compensation technique. *International Journal of Applied Engineering Research* **11**(10), 7139–7146 (2016)
9. Gong, Z., Yang, Z.: Video frame interpolation and extrapolation. Tech. rep., Stanford Univer-

- sity (2017). URL <http://cs231n.stanford.edu/reports/2017/pdfs/714.pdf>
10. Ha, T., Lee, S., Kim, J.: Motion compensated frame interpolation by new block-based motion estimation algorithm. *Transactions on Consumer Electronics (T-CE)* **50**(2), 752–759 (2004)
 11. Harel, J., Koch, C., Perona, P.: Graph-based visual saliency. In: *Advances in Neural Information Processing Systems*, pp. 545–552 (2007)
 12. Hoßfeld, T., Heegaard, P.E., Varela, M., Möller, S.: QoE beyond the MOS: an in-depth look at QoE via better metrics and their relation to MOS. *Quality and User Experience* **1**(2), 1–23 (2016)
 13. ITU-T Recommendation, P.: Subjective video quality assessment methods for multimedia applications. Tech. rep. (1999). URL <https://www.itu.int/rec/T-REC-P.910-200804-I>
 14. Jiang, H., Sun, D., Jampani, V., Yang, M.H., Learned-Miller, E., Kautz, J.: Super slomo: High quality estimation of multiple intermediate frames for video interpolation. In: *Computer Vision and Pattern Recognition (CVPR)*, pp. 9000–9008 (2018)
 15. Larson, E.C., Chandler, D.M.: Most apparent distortion: full-reference image quality assessment and the role of strategy. *Journal of Electronic Imaging* **19**(1), 011006 (2010)
 16. Liu, Y.L., Liao, Y.T., Lin, Y.Y., Chuang, Y.Y.: Deep video frame interpolation using cyclic frame generation. In: *AAAI Conference on Artificial Intelligence* (2019)
 17. Liu, Z., Yeh, R.A., Tang, X., Liu, Y., Agarwala, A.: Video frame synthesis using deep voxel flow. In: *International Conference on Computer Vision (ICCV)*, pp. 4463–4471 (2017)
 18. Luce, R.D.: Thurstone and sensory scaling: Then and now. *US: American Psychological Association* **101**(2), 271–277 (1994)
 19. Masia, B., Serrano, A., Gutierrez, D.: Dynamic range expansion based on image statistics. *Multimedia Tools and Applications* **76**(1), 631–648 (2017)
 20. McCann, J., Pollard, N.S., Srinivasa, S.: Physics-based motion retiming. In: *Eurographics (EG) / ACM SIGGRAPH Symposium on Computer Animation*, pp. 205–214 (2006)
 21. Men, H., Lin, H., Hosu, V., Maurer, D., Bruhn, A., Saupé, D.: Visual quality assessment for motion compensated frame interpolation. In: *International Conference on Quality of Multimedia Experience (QoMEX)*, pp. 1–6. IEEE (2019)
 22. Meyer, S., Wang, O., Zimmer, H., Grosse, M., Sorkine-Hornung, A.: Phase-based frame interpolation for video. In: *Computer Vision and Pattern Recognition (CVPR)*, pp. 1410–1418. IEEE (2015)
 23. Niklaus, S., Liu, F.: Context-aware synthesis for video frame interpolation. In: *Computer Vision and Pattern Recognition (CVPR)*, pp. 1701–1710. IEEE (2018)
 24. Otsu, N.: A threshold selection method from gray-level histograms. *IEEE Transactions on Systems, Man, and Cybernetics* **9**(1), 62–66 (1979)
 25. Prochwicz, K.: Semantic satiation in schizophrenia: the role of valence of stimuli. *Archives of Psychiatry and Psychotherapy* **4**, 23–29 (2010)
 26. Rakét, L.L., Roholm, L., Bruhn, A., Weickert, J.: Motion compensated frame interpolation with a symmetric optical flow constraint. In: *International Symposium on Visual Computing*, pp. 447–457. Springer (2012)
 27. Ruscio, J.: Constructing confidence intervals for spearman's rank correlation with ordinal data: a simulation study comparing analytic and bootstrap methods. *Journal of Modern Applied Statistical Methods* **7**(2), 7 (2008)
 28. Saupé, D., Hahn, F., Hosu, V., Zingman, I., Rana, M., Li, S.: Crowd workers proven useful: A comparative study of subjective video quality assessment. In: *International Conference on Quality of Multimedia Experience (QoMEX)* (2016)
 29. Sheikh, H.R., Sabir, M.F., Bovik, A.C.: A statistical evaluation of recent full reference image quality assessment algorithms. *IEEE Transactions on Image Processing (TIP)* **15**(11), 3440–3451 (2006)
 30. Soomro, K., Zamir, A.R., Shah, M.: UCF101: A dataset of 101 human actions classes from videos in the wild. *arXiv e-prints arXiv:1212.0402* (2012)
 31. Thurstone, L.L.: A law of comparative judgment. *Psychological Review* **34**(4), 273 (1927)
 32. Tsukida, K., Gupta, M.R.: How to analyze paired comparison data. Tech. rep., University of Washington (2011). URL <https://www.itu.int/rec/T-REC-P.910-200804-I>
 33. VIPSL: (2005). <http://see.xidian.edu.cn/vips1/dataset.html>
 34. VIPSL: (2005). http://see.xidian.edu.cn/vips1/database_Video.html
 35. Wang, T.H., Chiu, C.T.: Low visual difference virtual high dynamic range image synthesizer from a single legacy image. In: *International Conference on Image Processing (ICIP)*, pp. 2265–2268 (2011)
 36. Wang, Z., Bovik, A.C., Sheikh, H.R., Simoncelli, E.P.: Image quality assessment: from error visibility to structural similarity. *IEEE Transactions on Image Processing (TIP)* **13**(4), 600–612 (2004)
 37. Wang, Z., Simoncelli, E.P., Bovik, A.C.: Multiscale structural similarity for image quality assessment. In: *IEEE Asilomar Conference on Signals, Systems & Computers*, vol. 2, pp. 1398–1402 (2003)

38. Xu, Q., Huang, Q., Jiang, T., Yan, B., Lin, W., Yao, Y.: Hodgerank on random graphs for subjective video quality assessment. *IEEE Transactions on Multimedia (TMM)* **14**(3), 844–857 (2012)
39. Xue, W., Zhang, L., Mou, X., Bovik, A.C.: Gradient magnitude similarity deviation: A highly efficient perceptual image quality index. *IEEE Transactions on Image Processing (TIP)* **23**(2), 684–695 (2014)
40. Zhai, J., Yu, K., Li, J., Li, S.: A low complexity motion compensated frame interpolation method. In: *International Symposium on Circuits and Systems (ISCAS)*, pp. 4927–4930. Springer (2005)
41. Zhang, L., Gu, Z., Li, H.: SDSP: A novel saliency detection method by combining simple priors. In: *International Conference on Image Processing (ICIP)*, pp. 171–175. IEEE (2013)
42. Zhang, L., Shen, Y., Li, H.: VSI: A visual saliency-induced index for perceptual image quality assessment. *IEEE Transactions on Image Processing (TIP)* **23**(10), 4270–4281 (2014)
43. Zhang, L., Zhang, L., Mou, X., Zhang, D.: FSIM: a feature similarity index for image quality assessment. *IEEE Transactions on Image Processing (TIP)* **20**(8), 2378–2386 (2011)

Table 4 Subjective Quality Values and the Re-ranking of the Middlebury Benchmark (Part I)

	Average	Mequon	Schefflera	Urban	Teddy	Backyard	Basketball	Dumptruck	Evergreen
CtxSyn	0.771 / 1	0.918 / 1	0.699 / 29	0.658 / 45	0.781 / 2	0.767 / 16	0.666 / 26	0.877 / 5	0.804 / 1
CyclicGen	0.758 / 2	0.868 / 2	0.500 / 81	0.877 / 3	0.832 / 1	0.798 / 13	0.644 / 35	0.778 / 12	0.767 / 2
SuperSloMo	0.754 / 3	0.814 / 4	0.699 / 30	0.908 / 2	0.564 / 54	0.654 / 38	0.729 / 14	0.984 / 1	0.677 / 12
TOFM	0.732 / 4	0.802 / 5	0.443 / 92	0.736 / 22	0.663 / 17	0.891 / 2	0.759 / 10	0.902 / 4	0.661 / 18
FMO-F	0.727 / 5	0.744 / 11	0.627 / 55	0.606 / 59	0.600 / 39	0.872 / 7	0.783 / 6	0.912 / 3	0.675 / 14
MEMC-Net+	0.721 / 6	0.837 / 3	0.724 / 26	0.340 / 115	0.726 / 5	0.735 / 20	0.847 / 2	0.790 / 10	0.766 / 3
SepConv-v1	0.713 / 7	0.798 / 6	0.560 / 69	0.606 / 60	0.596 / 41	0.675 / 31	0.863 / 1	0.854 / 6	0.755 / 4
MDP-Flow2	0.712 / 8	0.654 / 24	0.878 / 5	0.800 / 8	0.610 / 33	0.884 / 4	0.582 / 55	0.649 / 41	0.639 / 23
CBF	0.707 / 9	0.627 / 31	0.514 / 77	0.744 / 20	0.769 / 3	0.987 / 1	0.773 / 7	0.549 / 69	0.693 / 9
PMMST	0.692 / 10	0.607 / 36	0.836 / 9	0.725 / 29	0.683 / 10	0.732 / 21	0.796 / 4	0.571 / 62	0.586 / 45
AdaConv-v1	0.682 / 11	0.490 / 84	0.777 / 16	0.673 / 39	0.572 / 53	0.883 / 5	0.757 / 11	0.571 / 61	0.735 / 6
Second-order prior	0.668 / 12	0.754 / 7	0.376 / 107	0.684 / 35	0.741 / 4	0.656 / 36	0.768 / 9	0.739 / 21	0.621 / 32
SuperFlow	0.664 / 13	0.706 / 15	0.629 / 53	0.614 / 55	0.589 / 45	0.876 / 6	0.692 / 21	0.645 / 44	0.558 / 54
NNF-Local	0.653 / 14	0.698 / 17	0.862 / 6	0.730 / 26	0.350 / 133	0.803 / 12	0.508 / 84	0.656 / 40	0.620 / 34
LDOF	0.653 / 15	0.577 / 45	0.733 / 24	0.479 / 85	0.602 / 37	0.841 / 9	0.720 / 16	0.771 / 13	0.503 / 76
Aniso-Texture	0.652 / 16	0.693 / 18	0.396 / 103	0.670 / 40	0.700 / 8	0.662 / 34	0.638 / 37	0.804 / 9	0.656 / 19
ALD-Flow	0.651 / 17	0.376 / 126	0.643 / 48	0.786 / 11	0.614 / 30	0.819 / 11	0.659 / 27	0.768 / 14	0.539 / 62
Brox et al.	0.649 / 18	0.399 / 118	0.696 / 31	0.641 / 48	0.681 / 11	0.850 / 8	0.525 / 76	0.752 / 17	0.650 / 20
CLG-TV	0.647 / 19	0.499 / 78	0.276 / 123	0.693 / 34	0.719 / 6	0.659 / 35	0.718 / 18	0.935 / 2	0.679 / 11
DeepFlow	0.643 / 20	0.566 / 48	0.503 / 79	0.683 / 36	0.531 / 70	0.684 / 29	0.834 / 3	0.730 / 23	0.614 / 36
WLIF-Flow	0.637 / 21	0.740 / 12	0.754 / 20	0.566 / 68	0.598 / 40	0.753 / 19	0.482 / 92	0.649 / 42	0.548 / 58
LME	0.632 / 22	0.753 / 8	0.679 / 36	0.576 / 65	0.660 / 19	0.545 / 64	0.493 / 89	0.703 / 27	0.644 / 22
DeepFlow2	0.626 / 23	0.545 / 57	0.551 / 72	0.780 / 12	0.523 / 76	0.579 / 57	0.785 / 5	0.636 / 48	0.607 / 40
Modified CLG	0.618 / 24	0.645 / 25	0.193 / 142	0.733 / 24	0.602 / 36	0.769 / 15	0.584 / 54	0.814 / 7	0.604 / 41
Bartels	0.615 / 25	0.450 / 99	0.567 / 65	0.744 / 19	0.506 / 82	0.710 / 23	0.573 / 57	0.755 / 16	0.611 / 38
SIOF	0.615 / 26	0.460 / 97	0.407 / 100	0.654 / 47	0.638 / 24	0.884 / 3	0.646 / 32	0.741 / 20	0.485 / 87
CombBMOF	0.612 / 27	0.377 / 125	0.859 / 7	0.710 / 33	0.584 / 49	0.441 / 96	0.650 / 31	0.542 / 70	0.736 / 5
IROF++	0.610 / 28	0.664 / 23	0.690 / 33	0.629 / 53	0.606 / 35	0.513 / 75	0.738 / 13	0.641 / 46	0.401 / 127
DPOF	0.606 / 29	0.588 / 43	0.764 / 19	0.495 / 83	0.668 / 15	0.693 / 27	0.573 / 58	0.420 / 101	0.645 / 21
P-harmonic	0.604 / 30	0.672 / 21	0.326 / 115	0.735 / 23	0.563 / 55	0.600 / 49	0.602 / 47	0.722 / 26	0.613 / 37
EAI-Flow	0.604 / 31	0.470 / 95	0.627 / 54	0.595 / 62	0.607 / 34	0.477 / 86	0.654 / 30	0.765 / 15	0.634 / 28
NNF-EAC	0.603 / 32	0.553 / 55	0.748 / 22	0.576 / 66	0.544 / 63	0.541 / 67	0.772 / 8	0.490 / 82	0.599 / 42
3DFlow	0.601 / 33	0.505 / 73	0.667 / 43	0.639 / 49	0.708 / 7	0.670 / 33	0.383 / 115	0.601 / 57	0.638 / 25
NN-field	0.601 / 34	0.749 / 9	0.922 / 2	0.353 / 113	0.290 / 145	0.695 / 26	0.628 / 39	0.534 / 72	0.635 / 27
PH-Flow	0.599 / 35	0.487 / 85	0.889 / 4	0.725 / 30	0.684 / 9	0.599 / 50	0.239 / 144	0.605 / 55	0.563 / 52
OAR-Flow	0.598 / 36	0.556 / 53	0.585 / 63	0.844 / 4	0.510 / 79	0.560 / 59	0.550 / 68	0.688 / 32	0.492 / 82
MLDP_OF	0.591 / 37	0.613 / 34	0.514 / 76	0.753 / 17	0.524 / 74	0.495 / 81	0.535 / 70	0.689 / 31	0.607 / 39
MDP-Flow	0.587 / 38	0.704 / 16	0.766 / 18	0.631 / 52	0.446 / 110	0.473 / 90	0.277 / 134	0.722 / 25	0.675 / 13
LFNet_ROB	0.586 / 39	0.421 / 110	0.689 / 34	0.666 / 41	0.633 / 25	0.345 / 119	0.590 / 49	0.806 / 8	0.539 / 61
JOE	0.581 / 40	0.592 / 39	0.695 / 32	0.757 / 16	0.612 / 32	0.443 / 95	0.318 / 129	0.724 / 24	0.506 / 74
ComplOF-FED-GPU	0.577 / 41	0.481 / 87	0.627 / 56	0.327 / 120	0.670 / 14	0.582 / 56	0.644 / 34	0.751 / 18	0.531 / 65
NL-TV-NCC	0.572 / 42	0.495 / 80	0.667 / 44	0.730 / 25	0.382 / 122	0.757 / 18	0.434 / 100	0.614 / 53	0.498 / 78
Classic++	0.565 / 43	0.727 / 14	0.474 / 87	0.682 / 37	0.416 / 113	0.603 / 48	0.686 / 22	0.298 / 123	0.637 / 26
FC-2Layers-FF	0.564 / 44	0.430 / 105	0.268 / 127	0.804 / 7	0.540 / 65	0.558 / 61	0.700 / 20	0.492 / 80	0.718 / 7
IROF-TV	0.560 / 45	0.477 / 89	0.688 / 35	0.633 / 51	0.531 / 71	0.595 / 52	0.533 / 71	0.553 / 66	0.469 / 95
FOLKI	0.559 / 46	0.432 / 104	0.502 / 80	0.332 / 118	0.516 / 77	0.761 / 17	0.681 / 23	0.684 / 33	0.565 / 50
DF-Auto	0.557 / 47	0.405 / 115	0.371 / 109	0.808 / 5	0.614 / 31	0.676 / 30	0.559 / 65	0.511 / 76	0.513 / 70
BlockOverlap	0.553 / 48	0.591 / 40	0.439 / 94	0.338 / 116	0.541 / 64	0.710 / 24	0.444 / 98	0.669 / 38	0.689 / 10
TC-Flow	0.550 / 49	0.425 / 109	0.507 / 78	0.729 / 27	0.562 / 56	0.517 / 72	0.673 / 25	0.566 / 64	0.423 / 116
TCOF	0.547 / 50	0.401 / 117	0.638 / 52	0.675 / 38	0.487 / 94	0.514 / 74	0.633 / 38	0.536 / 71	0.495 / 79
Fusion	0.546 / 51	0.592 / 38	0.754 / 21	0.797 / 9	0.419 / 112	0.539 / 68	0.406 / 108	0.336 / 112	0.527 / 67
RNLOD-Flow	0.546 / 52	0.624 / 32	0.517 / 75	0.658 / 44	0.616 / 29	0.285 / 128	0.555 / 67	0.642 / 45	0.475 / 90
Layers++	0.545 / 53	0.682 / 20	0.920 / 3	0.433 / 95	0.676 / 12	0.195 / 145	0.289 / 133	0.647 / 43	0.522 / 68
TF+OM	0.545 / 54	0.428 / 107	0.641 / 50	0.587 / 64	0.501 / 85	0.582 / 55	0.679 / 24	0.446 / 93	0.499 / 77
2DHMM-SAS	0.543 / 55	0.603 / 37	0.380 / 106	0.492 / 84	0.620 / 27	0.383 / 109	0.656 / 29	0.618 / 52	0.595 / 43
FF++_ROB	0.543 / 56	0.457 / 98	0.775 / 17	0.609 / 58	0.589 / 46	0.477 / 85	0.585 / 52	0.387 / 105	0.468 / 97
Occlusion-TV-L1	0.541 / 57	0.521 / 65	0.327 / 114	0.963 / 1	0.346 / 134	0.609 / 45	0.471 / 96	0.657 / 39	0.437 / 113
nLayers	0.539 / 58	0.620 / 33	0.821 / 11	0.473 / 88	0.470 / 100	0.226 / 138	0.403 / 110	0.669 / 37	0.631 / 29
HAST	0.536 / 59	0.540 / 61	0.784 / 14	0.526 / 79	0.661 / 18	0.417 / 103	0.403 / 109	0.492 / 81	0.466 / 100
Local-TV-L1	0.532 / 60	0.553 / 56	0.154 / 146	0.806 / 6	0.640 / 23	0.493 / 82	0.432 / 101	0.474 / 86	0.702 / 8
AggregFlow	0.529 / 61	0.304 / 140	0.674 / 40	0.570 / 67	0.488 / 92	0.642 / 41	0.646 / 33	0.353 / 110	0.553 / 57
TC/T-Flow	0.528 / 62	0.502 / 75	0.431 / 96	0.538 / 75	0.642 / 21	0.721 / 22	0.656 / 28	0.289 / 128	0.446 / 108
AGIF+OF	0.527 / 63	0.328 / 136	0.425 / 97	0.759 / 15	0.620 / 28	0.473 / 91	0.594 / 48	0.564 / 65	0.455 / 102
ACK-Prior	0.523 / 64	0.478 / 88	0.717 / 28	0.286 / 126	0.523 / 75	0.473 / 89	0.639 / 36	0.483 / 83	0.588 / 44
ComponentFusion	0.516 / 65	0.438 / 103	0.853 / 8	0.426 / 96	0.595 / 42	0.492 / 83	0.500 / 86	0.329 / 117	0.492 / 83
FlowNetS+ft+v	0.515 / 66	0.513 / 69	0.248 / 130	0.746 / 18	0.671 / 13	0.537 / 69	0.621 / 42	0.294 / 126	0.492 / 84
Filter Flow	0.513 / 67	0.476 / 91	0.293 / 120	0.426 / 97	0.486 / 95	0.671 / 32	0.587 / 50	0.609 / 54	0.554 / 56
Sparse Occlusion	0.511 / 68	0.573 / 46	0.490 / 84	0.633 / 50	0.586 / 48	0.605 / 47	0.316 / 130	0.434 / 95	0.454 / 104
COFM	0.510 / 69	0.351 / 131	0.623 / 58	0.787 / 10	0.591 / 44	0.475 / 87	0.229 / 146	0.451 / 91	0.574 / 48
Ad-TV-NDC	0.509 / 70	0.427 / 108	0.003 / 155	0.728 / 28	0.578 / 52	0.522 / 71	0.472 / 95	0.682 / 34	0.663 / 17
TI-DOFE	0.509 / 71	0.439 / 102	0.144 / 148	0.663 / 42	0.356 / 132	0.685 / 28	0.628 / 40	0.691 / 30	0.468 / 98
Steered-L1	0.506 / 72	0.630 / 29	0.640 / 51	0.206 / 137	0.452 / 106	0.613 / 44	0.509 / 81	0.552 / 68	0.445 / 110
CRTflow	0.504 / 73	0.430 / 106	0.318 / 116	0.616 / 54	0.621 / 26	0.509 / 76	0.707 / 19	0.206 / 145	0.624 / 30
FlowFields	0.504 / 74	0.544 / 58	0.795 / 13	0.414 / 102	0.490 / 90	0.379 / 111	0.486 / 91	0.534 / 73	0.387 / 130
BriefMatch	0.501 / 75	0.413 / 114	0.659 / 45	0.398 / 104	0.272 / 147	0.507 / 77	0.432 / 102	0.783 / 11	0.546 / 59
CPM-Flow	0.501 / 76	0.501 / 76	0.748 / 23	0.223 / 133	0.472 / 99	0.349 / 118	0.605 / 46	0.468 / 88	0.638 / 24
AugFNG_ROB	0.498 / 77	0.560 / 52	0.462 / 89	0.535 / 76	0.359 / 131	0.369 / 113	0.613 / 43	0.475 / 85	0.615 / 35

Table 5 Subjective Quality Values and the Re-ranking of the Middlebury Benchmark (Part II)

	Average	Mequon	Schefflera	Urban	Teddy	Backyard	Basketball	Dumptruck	Evergreen
S2F-IF	0.494 / 78	0.346 / 132	0.723 / 27	0.359 / 112	0.458 / 104	0.416 / 105	0.463 / 97	0.623 / 51	0.565 / 51
ResPWCROB	0.494 / 79	0.383 / 123	0.566 / 67	0.560 / 70	0.307 / 142	0.415 / 106	0.752 / 12	0.553 / 67	0.415 / 119
TV-L1-MCT	0.494 / 80	0.501 / 77	0.473 / 88	0.531 / 77	0.536 / 68	0.241 / 134	0.416 / 105	0.680 / 35	0.573 / 49
CNN-flow-warp+ref	0.491 / 81	0.746 / 10	0.363 / 110	0.547 / 74	0.449 / 107	0.542 / 65	0.337 / 125	0.322 / 119	0.623 / 31
FlowFields+	0.490 / 82	0.566 / 49	0.674 / 39	0.515 / 80	0.413 / 114	0.441 / 97	0.351 / 121	0.510 / 77	0.450 / 106
DMF_ROB	0.487 / 83	0.484 / 86	0.357 / 111	0.590 / 63	0.551 / 60	0.289 / 126	0.520 / 78	0.528 / 74	0.578 / 46
TriFlow	0.487 / 84	0.442 / 101	0.475 / 86	0.657 / 46	0.381 / 124	0.338 / 120	0.572 / 59	0.576 / 60	0.452 / 105
FESL	0.486 / 85	0.520 / 66	0.923 / 1	0.659 / 43	0.582 / 50	0.240 / 135	0.139 / 152	0.317 / 120	0.505 / 75
FlowNet2	0.485 / 86	0.186 / 152	0.778 / 15	0.417 / 100	0.370 / 130	0.632 / 43	0.546 / 69	0.396 / 103	0.555 / 55
SVFilterOh	0.484 / 87	0.395 / 119	0.824 / 10	0.323 / 121	0.588 / 47	0.284 / 130	0.532 / 72	0.423 / 98	0.506 / 73
F-TV-L1	0.481 / 88	0.387 / 121	0.183 / 143	0.344 / 114	0.377 / 126	0.835 / 10	0.560 / 64	0.700 / 28	0.465 / 101
OFH	0.481 / 89	0.634 / 28	0.437 / 95	0.378 / 109	0.507 / 80	0.417 / 104	0.586 / 51	0.475 / 84	0.412 / 121
2D-CLG	0.479 / 90	0.737 / 13	0.236 / 135	0.551 / 73	0.560 / 57	0.449 / 93	0.354 / 120	0.371 / 108	0.575 / 47
PWCNet_ROB	0.478 / 91	0.302 / 141	0.624 / 57	0.771 / 14	0.327 / 138	0.232 / 137	0.495 / 87	0.679 / 36	0.397 / 128
EPM w/o HM	0.478 / 92	0.476 / 92	0.731 / 25	0.065 / 154	0.479 / 98	0.700 / 25	0.565 / 60	0.295 / 125	0.511 / 72
PMF	0.476 / 93	0.588 / 42	0.500 / 82	0.174 / 141	0.559 / 58	0.586 / 54	0.623 / 41	0.366 / 109	0.414 / 120
OFLAF	0.473 / 94	0.630 / 30	0.803 / 12	0.609 / 57	0.581 / 51	0.103 / 155	0.272 / 137	0.379 / 107	0.409 / 122
TriangleFlow	0.472 / 95	0.490 / 83	0.559 / 70	0.554 / 72	0.557 / 59	0.635 / 42	0.575 / 56	0.091 / 153	0.312 / 140
PGM-C	0.465 / 96	0.523 / 64	0.671 / 41	0.332 / 119	0.410 / 115	0.331 / 121	0.561 / 63	0.461 / 90	0.431 / 115
Adaptive	0.464 / 97	0.670 / 22	0.268 / 126	0.564 / 69	0.527 / 73	0.516 / 73	0.303 / 132	0.325 / 118	0.540 / 60
Horn&Schunck	0.463 / 98	0.590 / 41	0.248 / 129	0.188 / 139	0.342 / 136	0.656 / 37	0.524 / 77	0.630 / 50	0.531 / 66
GraphCuts	0.462 / 99	0.332 / 135	0.619 / 59	0.229 / 132	0.514 / 78	0.448 / 94	0.509 / 82	0.580 / 59	0.467 / 99
Sparse-NonSparse	0.462 / 100	0.519 / 67	0.649 / 47	0.529 / 78	0.536 / 67	0.286 / 127	0.268 / 138	0.421 / 99	0.486 / 86
Rflow	0.460 / 101	0.689 / 19	0.275 / 124	0.386 / 105	0.461 / 103	0.558 / 60	0.344 / 124	0.498 / 79	0.469 / 96
HBM-GC	0.458 / 102	0.535 / 63	0.549 / 73	0.446 / 92	0.591 / 43	0.193 / 146	0.264 / 140	0.420 / 100	0.666 / 15
UnFlow	0.455 / 103	0.379 / 124	0.399 / 101	0.507 / 81	0.649 / 20	0.498 / 79	0.274 / 136	0.744 / 19	0.194 / 150
CostFilter	0.455 / 104	0.562 / 51	0.675 / 37	0.306 / 125	0.493 / 89	0.361 / 114	0.606 / 44	0.279 / 130	0.357 / 134
Nguyen	0.451 / 105	0.402 / 116	0.053 / 153	0.775 / 13	0.503 / 83	0.609 / 46	0.562 / 62	0.218 / 142	0.485 / 89
Classic+CPF	0.450 / 106	0.472 / 94	0.567 / 66	0.321 / 122	0.663 / 16	0.425 / 100	0.363 / 118	0.315 / 121	0.475 / 91
Complementary OF	0.447 / 107	0.419 / 112	0.674 / 38	0.128 / 149	0.401 / 120	0.556 / 62	0.526 / 75	0.588 / 58	0.284 / 144
EPMNet	0.445 / 108	0.255 / 145	0.643 / 49	0.452 / 91	0.337 / 137	0.597 / 51	0.413 / 106	0.426 / 97	0.440 / 111
LiteFlowNet	0.441 / 109	0.497 / 79	0.591 / 61	0.420 / 99	0.381 / 123	0.313 / 123	0.388 / 114	0.467 / 89	0.474 / 92
Ramp	0.439 / 110	0.506 / 72	0.670 / 42	0.379 / 108	0.600 / 38	0.284 / 129	0.242 / 142	0.385 / 106	0.449 / 107
Dynamic MRF	0.436 / 111	0.644 / 26	0.457 / 90	0.560 / 71	0.408 / 117	0.643 / 40	0.127 / 153	0.249 / 136	0.403 / 126
EpicFlow	0.435 / 112	0.463 / 96	0.556 / 71	0.473 / 89	0.454 / 105	0.293 / 125	0.482 / 93	0.420 / 102	0.336 / 136
ProbFlowFields	0.434 / 113	0.567 / 47	0.616 / 60	0.409 / 103	0.507 / 81	0.213 / 139	0.266 / 139	0.332 / 115	0.560 / 53
Black & Anandan	0.433 / 114	0.295 / 143	0.301 / 119	0.222 / 134	0.408 / 116	0.650 / 39	0.493 / 88	0.431 / 96	0.664 / 16
Aniso.Huber-L1	0.430 / 115	0.509 / 71	0.398 / 102	0.741 / 21	0.321 / 141	0.428 / 99	0.303 / 131	0.273 / 131	0.470 / 94
Learning Flow	0.428 / 116	0.610 / 35	0.269 / 125	0.135 / 148	0.487 / 93	0.418 / 102	0.530 / 73	0.570 / 63	0.408 / 123
HbpMotionGpu	0.419 / 117	0.186 / 151	0.587 / 62	0.414 / 101	0.298 / 143	0.792 / 14	0.354 / 119	0.446 / 94	0.274 / 146
FFV1MT	0.416 / 118	0.475 / 93	0.497 / 83	0.370 / 111	0.482 / 97	0.236 / 136	0.348 / 123	0.448 / 92	0.474 / 93
Efficient-NL	0.415 / 119	0.580 / 44	0.441 / 93	0.386 / 107	0.529 / 72	0.361 / 115	0.274 / 135	0.217 / 143	0.531 / 64
LSM	0.414 / 120	0.450 / 100	0.568 / 64	0.505 / 82	0.494 / 88	0.155 / 151	0.378 / 116	0.251 / 135	0.511 / 71
HCIC-L	0.411 / 121	0.321 / 137	0.130 / 150	0.718 / 31	0.273 / 146	0.382 / 110	0.349 / 122	0.731 / 22	0.387 / 129
Classic+NL	0.411 / 122	0.564 / 50	0.485 / 85	0.442 / 93	0.641 / 22	0.154 / 152	0.319 / 128	0.188 / 148	0.494 / 80
LocallyOriented	0.410 / 123	0.491 / 82	0.292 / 121	0.312 / 124	0.463 / 102	0.357 / 116	0.400 / 111	0.474 / 87	0.489 / 85
TVL1_ROB	0.407 / 124	0.639 / 27	0.205 / 139	0.146 / 146	0.540 / 66	0.593 / 53	0.324 / 127	0.297 / 124	0.515 / 69
Correlation Flow	0.406 / 125	0.492 / 81	0.382 / 104	0.716 / 32	0.405 / 119	0.392 / 108	0.207 / 149	0.202 / 147	0.455 / 103
S2D-Matching	0.406 / 126	0.356 / 129	0.415 / 98	0.612 / 56	0.549 / 62	0.195 / 144	0.328 / 126	0.390 / 104	0.404 / 125
SLK	0.402 / 127	0.543 / 59	0.233 / 136	0.221 / 135	0.377 / 127	0.527 / 70	0.723 / 15	0.310 / 122	0.281 / 145
SRR-TVOF-NL	0.402 / 128	0.386 / 122	0.565 / 68	0.260 / 129	0.501 / 86	0.159 / 150	0.397 / 112	0.528 / 75	0.418 / 117
ROF-ND	0.399 / 129	0.477 / 90	0.411 / 99	0.599 / 61	0.159 / 152	0.196 / 143	0.396 / 113	0.641 / 47	0.311 / 141
OFRF	0.393 / 130	0.334 / 134	0.166 / 145	0.467 / 90	0.490 / 91	0.257 / 132	0.720 / 17	0.289 / 127	0.417 / 118
SILK	0.389 / 131	0.353 / 130	0.141 / 149	0.074 / 153	0.322 / 139	0.542 / 66	0.563 / 61	0.633 / 49	0.485 / 88
SegOF	0.388 / 132	0.538 / 62	0.520 / 74	0.159 / 143	0.264 / 148	0.495 / 80	0.509 / 83	0.332 / 114	0.287 / 143
IAOF2	0.387 / 133	0.540 / 60	0.238 / 134	0.434 / 94	0.344 / 135	0.270 / 131	0.492 / 90	0.331 / 116	0.445 / 109
StereoFlow	0.383 / 134	0.220 / 149	0.355 / 112	0.476 / 87	0.366 / 69	0.401 / 107	0.241 / 143	0.503 / 78	0.329 / 138
H+S_ROB	0.375 / 135	0.512 / 70	0.316 / 117	0.199 / 138	0.374 / 128	0.551 / 63	0.407 / 107	0.270 / 132	0.370 / 133
PGAM+LK	0.374 / 136	0.295 / 142	0.182 / 144	0.178 / 140	0.163 / 151	0.469 / 92	0.606 / 45	0.694 / 29	0.406 / 124
FGIK	0.373 / 137	0.226 / 148	0.374 / 108	0.386 / 106	0.483 / 96	0.562 / 58	0.585 / 53	0.204 / 146	0.163 / 154
Rannacher	0.370 / 138	0.513 / 68	0.199 / 140	0.162 / 142	0.549 / 61	0.439 / 98	0.515 / 79	0.150 / 149	0.436 / 114
ContinualFlow_ROB	0.369 / 139	0.554 / 54	0.658 / 46	0.229 / 131	0.298 / 144	0.213 / 140	0.481 / 94	0.246 / 138	0.273 / 147
Shiralkar	0.358 / 140	0.390 / 120	0.309 / 118	0.253 / 130	0.371 / 129	0.478 / 84	0.514 / 80	0.239 / 139	0.313 / 139
IIOF-NLDP	0.348 / 141	0.413 / 113	0.451 / 91	0.336 / 117	0.448 / 109	0.473 / 88	0.223 / 147	0.058 / 154	0.379 / 131
TV-L1-improved	0.347 / 142	0.314 / 138	0.211 / 138	0.375 / 110	0.429 / 111	0.313 / 122	0.440 / 99	0.256 / 134	0.440 / 112
StereoOF-V1MT	0.343 / 143	0.357 / 128	0.240 / 133	0.155 / 144	0.380 / 125	0.354 / 117	0.419 / 103	0.347 / 111	0.494 / 81
2bit-BM-tele	0.338 / 144	0.310 / 139	0.284 / 122	0.477 / 86	0.498 / 87	0.187 / 147	0.206 / 150	0.120 / 150	0.621 / 33
IAOF	0.322 / 145	0.233 / 147	0.150 / 147	0.113 / 151	0.407 / 118	0.421 / 101	0.501 / 85	0.221 / 141	0.531 / 63
Pyramid LK	0.301 / 146	0.375 / 127	0.197 / 141	0.316 / 123	0.127 / 153	0.504 / 78	0.528 / 74	0.285 / 129	0.075 / 155
Adaptive flow	0.299 / 147	0.244 / 146	0.095 / 151	0.420 / 98	0.233 / 149	0.210 / 142	0.235 / 145	0.604 / 56	0.351 / 135
SimpleFlow	0.294 / 148	0.503 / 74	0.381 / 105	0.105 / 152	0.502 / 84	0.183 / 148	0.221 / 148	0.120 / 151	0.334 / 137
Heeger++	0.284 / 149	0.159 / 153	0.332 / 113	0.269 / 128	0.448 / 108	0.176 / 149	0.373 / 117	0.333 / 113	0.184 / 152
SPSA-learn	0.282 / 150	0.341 / 133	0.243 / 132	0.147 / 145	0.399 / 121	0.372 / 112	0.260 / 141	0.247 / 137	0.244 / 148
WOLF_ROB	0.277 / 151	0.139 / 155	0.218 / 137	0.210 / 136	0.322 / 140	0.211 / 141	0.557 / 66	0.258 / 133	0.302 / 142
WRT	0.263 / 152	0.420 / 111	0.243 / 131	0.138 / 147	0.467 / 101	0.295 / 124	0.149 / 151	0.207 / 144	0.185 / 151
GroupFlow	0.225 / 153	0.200 / 150	0.257 / 128	0.039 / 155	0.207 / 150	0.250 / 133	0.416 / 104	0.233 / 140	0.200 / 149
AVG_FLOW_ROB	0.170 / 154	0.289 / 144	0.082 / 152	0.278 / 127	0.093 / 154	0.144 / 154	0.039 / 155	0.056 / 155	0.376 / 132
Periodicity	0.102 / 155	0.151 / 154	0.032 / 154	0.125 / 150	0.033 / 155	0.146 / 153	0.055 / 154	0.106 / 152	0.170 / 153

Table 6 Re-ranking of the Middlebury Benchmark. new: re-ranking given by subjective study. old: ranking in the Middlebury benchmark (Part I).

	Average	Mequon	Schefflera	Urban	Teddy	Backyard	Basketball	Dumptruck	Evergreen
CtxSyn	1 / 2	1 / 2	29 / 1	45 / 82	2 / 1	16 / 2	26 / 2	5 / 4	1 / 5
CyclicGen	2 / 1	2 / 1	81 / 2	3 / 1	1 / 3	13 / 1	35 / 1	12 / 1	2 / 1
SuperSlomo	3 / 3	4 / 3	30 / 9	2 / 2	54 / 7	38 / 3	14 / 6	1 / 3	12 / 4
TOFM	4 / 5	5 / 5	92 / 13	22 / 3	17 / 8	2 / 21	10 / 5	4 / 12	18 / 7
FMO-F	5 / 38	11 / 85	55 / 18	59 / 88	39 / 75	7 / 17	6 / 72	3 / 52	14 / 56
MEMC-Net+	6 / 4	3 / 4	26 / 3	115 / 99	5 / 2	20 / 15	2 / 3	10 / 23	3 / 2
SepConv-v1	7 / 6	6 / 6	69 / 10	60 / 72	41 / 36	31 / 16	1 / 4	6 / 11	4 / 3
MDP-Flow2	8 / 10	24 / 15	5 / 20	8 / 25	33 / 12	4 / 9	55 / 23	41 / 17	23 / 35
CBF	9 / 7	31 / 9	77 / 58	20 / 4	3 / 4	1 / 4	7 / 13	69 / 10	9 / 10
PMMST	10 / 9	36 / 17	9 / 29	29 / 7	10 / 37	21 / 8	4 / 8	62 / 25	45 / 21
AdaConv-v1	11 / 44	84 / 125	16 / 99	39 / 108	53 / 132	5 / 35	11 / 9	61 / 47	6 / 12
Second-order prior	12 / 19	7 / 11	107 / 92	35 / 10	4 / 13	36 / 47	9 / 29	21 / 8	32 / 39
SuperFlow	13 / 11	15 / 29	53 / 72	55 / 48	45 / 11	6 / 7	21 / 26	44 / 40	54 / 13
NNF-Local	14 / 14	17 / 18	6 / 6	26 / 17	133 / 94	12 / 12	84 / 54	40 / 38	34 / 24
LDOF	15 / 21	45 / 23	24 / 76	85 / 62	37 / 17	9 / 6	16 / 58	13 / 75	76 / 18
Aniso-Texture	16 / 128	18 / 70	103 / 130	40 / 96	8 / 144	34 / 131	37 / 147	9 / 91	19 / 127
ALD-Flow	17 / 33	126 / 106	48 / 60	11 / 15	30 / 71	11 / 28	27 / 18	14 / 28	62 / 99
Brox et al.	18 / 35	118 / 49	31 / 51	48 / 34	11 / 10	8 / 30	76 / 81	17 / 85	20 / 11
CLG-TV	19 / 23	78 / 27	123 / 97	34 / 16	6 / 9	35 / 79	18 / 14	2 / 18	11 / 25
DeepFlow	20 / 29	48 / 41	79 / 64	36 / 18	70 / 34	29 / 67	3 / 19	23 / 15	36 / 47
WLIF-Flow	21 / 30	12 / 20	20 / 41	68 / 63	40 / 27	19 / 22	92 / 94	42 / 24	58 / 45
LME	22 / 36	8 / 16	36 / 43	65 / 37	19 / 26	64 / 89	89 / 43	27 / 22	22 / 48
DeepFlow2	23 / 25	57 / 39	72 / 63	12 / 12	76 / 23	57 / 45	5 / 16	48 / 33	40 / 49
Modified CLG	24 / 28	25 / 8	142 / 116	24 / 52	36 / 31	15 / 36	54 / 49	7 / 6	41 / 33
Bartels	25 / 31	99 / 126	65 / 75	19 / 24	82 / 66	23 / 11	57 / 105	16 / 16	38 / 65
SIOF	26 / 17	97 / 60	100 / 115	47 / 58	24 / 28	3 / 5	32 / 20	20 / 31	87 / 46
CombBMOF	27 / 18	125 / 71	7 / 22	33 / 42	49 / 48	96 / 25	31 / 34	70 / 32	5 / 31
IROF++	28 / 40	23 / 36	33 / 32	53 / 71	35 / 5	75 / 42	13 / 63	46 / 36	127 / 58
DPOF	29 / 46	43 / 105	19 / 7	83 / 103	15 / 80	27 / 43	58 / 79	101 / 26	21 / 61
P-harmonic	30 / 24	21 / 22	115 / 104	23 / 9	55 / 51	49 / 44	47 / 15	26 / 13	37 / 40
EAI-Flow	31 / 43	95 / 120	54 / 47	62 / 70	34 / 56	86 / 55	30 / 32	15 / 60	28 / 41
NNF-EAC	32 / 26	55 / 35	22 / 40	66 / 54	63 / 45	67 / 65	8 / 10	82 / 20	42 / 34
3DFlow	33 / 75	73 / 92	43 / 48	49 / 66	7 / 87	33 / 68	115 / 132	57 / 88	25 / 68
NN-field	34 / 79	9 / 61	2 / 146	113 / 45	145 / 98	26 / 62	39 / 69	72 / 124	27 / 28
PH-Flow	35 / 27	85 / 66	4 / 11	30 / 29	9 / 14	50 / 18	144 / 116	55 / 58	52 / 43
OAR-Flow	36 / 45	53 / 78	63 / 55	4 / 19	79 / 74	59 / 64	68 / 38	32 / 90	82 / 69
MLDP_OF	37 / 54	34 / 42	76 / 89	17 / 22	74 / 85	81 / 91	70 / 100	31 / 51	39 / 76
MDP-Flow	38 / 39	16 / 10	18 / 12	52 / 43	110 / 69	90 / 71	134 / 109	25 / 9	13 / 54
LFNet_ROB	39 / 81	110 / 133	34 / 62	41 / 86	25 / 52	119 / 58	49 / 139	8 / 45	61 / 92
JOE	40 / 41	39 / 57	32 / 15	16 / 30	32 / 38	95 / 76	129 / 103	24 / 21	74 / 59
CompIOF-FED-GPU	41 / 67	87 / 101	56 / 38	120 / 114	14 / 44	56 / 59	34 / 35	18 / 71	65 / 109
NL-TV-NCC	42 / 92	80 / 90	44 / 100	25 / 60	122 / 137	18 / 29	100 / 123	53 / 101	78 / 88
Classic++	43 / 53	14 / 32	87 / 81	37 / 14	113 / 55	48 / 100	22 / 83	123 / 82	26 / 71
FC-2Layers-FF	44 / 99	105 / 80	127 / 8	7 / 78	65 / 65	61 / 118	20 / 127	80 / 123	7 / 91
IROF-TV	45 / 34	89 / 58	35 / 52	51 / 23	71 / 15	52 / 54	71 / 51	66 / 50	95 / 20
FOLKI	46 / 104	104 / 124	80 / 150	118 / 112	77 / 138	17 / 81	23 / 55	33 / 55	50 / 44
DF-Auto	47 / 13	115 / 14	109 / 67	5 / 35	31 / 25	30 / 20	65 / 24	76 / 42	70 / 16
BlockOverlap	48 / 37	40 / 25	94 / 106	116 / 69	64 / 42	24 / 41	98 / 44	38 / 63	10 / 8
TC-Flow	49 / 55	109 / 107	78 / 74	27 / 11	56 / 91	72 / 77	25 / 59	64 / 53	116 / 119
TCOF	50 / 86	117 / 54	52 / 140	38 / 46	94 / 22	74 / 108	38 / 57	71 / 119	79 / 100
Fusion	51 / 52	38 / 31	21 / 42	9 / 50	112 / 68	68 / 85	108 / 104	112 / 49	67 / 96
RNLOD-Flow	52 / 69	32 / 55	75 / 79	44 / 79	29 / 29	128 / 109	67 / 99	45 / 62	90 / 106
Layers++	53 / 61	20 / 19	3 / 4	95 / 53	12 / 43	145 / 146	133 / 138	43 / 35	68 / 38
TF+OM	54 / 56	107 / 115	50 / 39	64 / 27	85 / 97	55 / 78	24 / 61	93 / 97	77 / 55
2DHMM-SAS	55 / 50	37 / 56	106 / 96	84 / 77	27 / 35	109 / 87	29 / 48	52 / 57	43 / 64
FF++_ROB	56 / 103	98 / 108	17 / 46	58 / 104	46 / 127	85 / 107	52 / 97	105 / 81	97 / 101
Occlusion-TV-L1	57 / 58	65 / 79	114 / 125	1 / 6	134 / 121	45 / 52	96 / 56	39 / 64	113 / 81
nLayers	58 / 71	33 / 34	11 / 14	88 / 124	100 / 63	138 / 111	110 / 87	37 / 34	29 / 51
HAST	59 / 114	61 / 26	14 / 17	79 / 134	18 / 46	103 / 56	109 / 141	81 / 115	100 / 95
Local-TV-L1	60 / 118	56 / 103	146 / 139	6 / 119	23 / 135	82 / 130	101 / 74	86 / 99	8 / 110
AggregFlow	61 / 51	140 / 139	40 / 66	67 / 61	92 / 102	41 / 19	33 / 22	110 / 116	57 / 85
TC/T-Flow	62 / 64	75 / 84	96 / 82	75 / 21	21 / 96	22 / 50	28 / 47	128 / 117	108 / 74
AGIF+OF	63 / 68	136 / 65	97 / 36	15 / 40	28 / 49	91 / 97	48 / 126	65 / 73	102 / 111
ACK-Prior	64 / 115	88 / 99	28 / 53	126 / 138	75 / 95	89 / 104	36 / 110	83 / 48	44 / 97
ComponentFusion	65 / 102	103 / 116	8 / 37	96 / 65	42 / 50	83 / 101	86 / 45	117 / 136	83 / 132
FlowNetS+ft+v	66 / 47	69 / 67	130 / 133	18 / 38	13 / 33	69 / 90	42 / 17	126 / 104	84 / 32
Filter Flow	67 / 22	91 / 38	120 / 117	97 / 47	95 / 81	32 / 14	50 / 42	54 / 27	56 / 23
Sparse Occlusion	68 / 59	46 / 76	84 / 94	50 / 20	48 / 39	47 / 110	130 / 33	95 / 103	104 / 90
COFM	69 / 42	131 / 48	58 / 21	10 / 31	44 / 54	87 / 26	146 / 131	91 / 86	48 / 52
Ad-TV-NDC	70 / 12	108 / 40	155 / 120	28 / 8	52 / 58	71 / 31	95 / 27	34 / 5	17 / 9
TI-DOFE	71 / 62	102 / 86	148 / 148	42 / 44	132 / 122	28 / 37	40 / 80	30 / 29	98 / 67
Steered-L1	72 / 126	29 / 46	51 / 61	137 / 141	106 / 130	44 / 95	81 / 66	68 / 89	110 / 103
CRTflow	73 / 57	106 / 77	116 / 114	54 / 51	26 / 30	76 / 46	19 / 31	145 / 110	30 / 77
FlowFields	74 / 60	58 / 87	13 / 30	102 / 102	90 / 89	111 / 32	91 / 98	73 / 54	130 / 104
BriefMatch	75 / 108	114 / 114	45 / 50	104 / 128	147 / 131	77 / 38	102 / 106	11 / 84	59 / 79
CPM-Flow	76 / 49	76 / 96	23 / 24	133 / 56	99 / 103	118 / 51	46 / 60	88 / 44	24 / 87
AugFNG_ROB	77 / 122	52 / 138	89 / 90	76 / 91	131 / 148	113 / 143	43 / 95	85 / 96	35 / 53

Table 7 Re-ranking of the Middlebury Benchmark. new: re-ranking given by subjective study. old: ranking in the Middlebury benchmark (Part II).

	Average	Mequon	Schefflera	Urban	Teddy	Backyard	Basketball	Dumptruck	Evergreen
S2F-IF	78 / 63	132 / 100	27 / 23	112 / 49	104 / 93	105 / 75	97 / 70	51 / 66	51 / 113
ResPwCR_ROB	79 / 127	123 / 128	67 / 93	70 / 81	142 / 145	106 / 140	12 / 137	67 / 77	119 / 140
TV-L1-MCT	80 / 48	77 / 72	88 / 68	77 / 83	68 / 47	134 / 125	105 / 30	35 / 74	49 / 30
CNN-flow-warp+ref	81 / 94	10 / 21	110 / 86	74 / 105	107 / 101	65 / 96	125 / 37	119 / 129	31 / 57
FlowFields+	82 / 74	49 / 69	39 / 25	80 / 101	114 / 108	97 / 57	121 / 91	77 / 70	106 / 107
DMF_ROB	83 / 65	86 / 91	111 / 73	63 / 118	60 / 72	126 / 48	78 / 39	74 / 46	46 / 82
TriFlow	84 / 88	101 / 140	86 / 108	46 / 36	124 / 118	120 / 84	59 / 111	60 / 69	105 / 66
FESL	85 / 93	66 / 75	1 / 33	43 / 76	50 / 70	135 / 124	152 / 101	120 / 112	75 / 102
FlowNet2	86 / 107	152 / 147	15 / 95	100 / 93	130 / 112	43 / 60	69 / 78	103 / 107	55 / 62
SVFilterOh	87 / 101	119 / 94	10 / 19	121 / 127	47 / 76	130 / 83	72 / 117	98 / 68	73 / 83
F-TV-L1	88 / 16	121 / 83	143 / 102	114 / 28	126 / 19	10 / 34	64 / 12	28 / 30	101 / 15
OFH	89 / 95	28 / 74	95 / 85	109 / 92	80 / 82	104 / 88	51 / 52	84 / 108	121 / 125
2D-CLG	90 / 77	13 / 13	135 / 119	73 / 111	57 / 86	93 / 121	120 / 21	108 / 109	47 / 29
PWCNet_ROB	91 / 105	141 / 131	57 / 78	14 / 33	138 / 125	137 / 139	87 / 122	36 / 59	128 / 129
EPPM w/o HM	92 / 117	92 / 102	25 / 65	154 / 136	98 / 111	25 / 23	60 / 129	125 / 127	72 / 108
PMF	93 / 72	42 / 53	82 / 56	141 / 115	58 / 73	54 / 27	41 / 73	109 / 100	120 / 116
OFLAF	94 / 91	30 / 50	12 / 16	57 / 26	51 / 20	155 / 129	137 / 82	107 / 137	122 / 112
TriangleFlow	95 / 119	83 / 82	70 / 105	72 / 85	59 / 60	42 / 119	56 / 76	153 / 135	140 / 149
PGM-C	96 / 85	64 / 97	41 / 28	119 / 109	115 / 104	121 / 69	63 / 41	90 / 87	115 / 120
Adaptive	97 / 70	22 / 63	126 / 128	69 / 32	73 / 53	73 / 122	132 / 65	118 / 98	60 / 60
Horn&Schunck	98 / 84	41 / 37	129 / 142	139 / 129	136 / 119	37 / 49	77 / 28	50 / 56	66 / 26
GraphCuts	99 / 120	135 / 136	59 / 44	132 / 139	78 / 90	94 / 86	82 / 71	59 / 102	99 / 117
Sparse-NonSparse	100 / 82	67 / 45	47 / 35	78 / 67	67 / 40	127 / 112	138 / 90	99 / 120	86 / 94
Rflow	101 / 100	19 / 73	124 / 109	105 / 107	103 / 92	60 / 66	124 / 67	79 / 113	96 / 86
HBM-GC	102 / 87	63 / 47	73 / 83	92 / 41	43 / 67	146 / 120	140 / 144	100 / 92	15 / 50
UnFlow	103 / 133	124 / 144	101 / 107	81 / 100	20 / 83	79 / 150	136 / 149	19 / 93	150 / 151
CostFilter	104 / 113	51 / 113	37 / 57	125 / 122	89 / 116	114 / 40	44 / 53	130 / 126	134 / 130
Nguyen	105 / 20	116 / 24	153 / 5	13 / 87	83 / 113	46 / 10	62 / 36	142 / 19	89 / 27
Classic+CPF	106 / 109	94 / 68	66 / 49	122 / 73	16 / 24	100 / 134	118 / 135	121 / 121	91 / 123
Complementary OF	107 / 134	112 / 129	38 / 69	149 / 146	120 / 123	62 / 80	75 / 50	58 / 105	144 / 145
EPMNet	108 / 131	145 / 150	49 / 88	91 / 94	137 / 152	51 / 61	106 / 118	97 / 106	111 / 118
LiteFlowNet	109 / 132	79 / 135	61 / 59	99 / 117	123 / 149	123 / 141	114 / 136	89 / 131	92 / 80
Ramp	110 / 96	72 / 59	42 / 34	108 / 106	38 / 32	129 / 105	142 / 114	106 / 111	107 / 84
Dynamic MRF	111 / 121	26 / 88	90 / 80	71 / 116	117 / 129	40 / 73	153 / 134	136 / 134	126 / 122
EpicFlow	112 / 89	96 / 98	71 / 54	89 / 68	105 / 120	125 / 70	93 / 46	102 / 83	136 / 133
ProbFlowFields	113 / 66	47 / 95	60 / 27	103 / 113	81 / 64	139 / 53	139 / 77	115 / 79	53 / 42
Black & Anandan	114 / 78	143 / 51	119 / 134	134 / 137	116 / 88	39 / 39	88 / 40	96 / 37	16 / 14
Aniso.Huber-L1	115 / 15	71 / 12	102 / 111	21 / 13	141 / 6	99 / 63	131 / 11	131 / 7	94 / 17
Learning Flow	116 / 141	35 / 44	125 / 122	148 / 154	93 / 105	102 / 138	73 / 86	63 / 67	123 / 115
HbpMotionGpu	117 / 90	151 / 134	62 / 141	101 / 80	143 / 124	14 / 106	119 / 89	94 / 14	146 / 98
FFV1MT	118 / 138	93 / 143	83 / 127	111 / 135	97 / 133	136 / 115	123 / 128	92 / 139	93 / 139
Efficient-NL	119 / 111	44 / 30	93 / 70	107 / 125	72 / 61	115 / 99	135 / 113	143 / 114	64 / 114
LSM	120 / 97	100 / 62	64 / 45	82 / 74	88 / 62	151 / 116	116 / 120	135 / 118	71 / 105
HCIC-L	121 / 139	137 / 149	150 / 149	31 / 121	146 / 143	110 / 24	122 / 152	22 / 132	129 / 142
Classic+NL	122 / 73	50 / 33	85 / 31	93 / 97	22 / 21	152 / 113	128 / 92	148 / 95	80 / 75
LocallyOriented	123 / 32	82 / 28	121 / 110	124 / 5	102 / 18	116 / 82	111 / 25	87 / 41	85 / 19
TVL1_ROB	124 / 76	27 / 89	139 / 147	146 / 90	66 / 107	53 / 33	127 / 64	124 / 125	69 / 22
Correlation Flow	125 / 124	81 / 93	104 / 126	32 / 39	119 / 100	108 / 117	149 / 148	147 / 143	103 / 126
S2D-Matching	126 / 83	129 / 81	98 / 77	56 / 95	62 / 59	144 / 94	126 / 130	104 / 78	125 / 72
SLK	127 / 149	59 / 117	136 / 131	135 / 149	127 / 146	70 / 147	15 / 84	122 / 142	145 / 137
SRR-TVOF-NL	128 / 80	122 / 111	68 / 71	129 / 98	86 / 99	150 / 93	112 / 107	75 / 43	117 / 93
ROF-ND	129 / 112	90 / 64	99 / 91	61 / 55	152 / 139	143 / 92	113 / 125	47 / 65	141 / 138
ORF	130 / 123	134 / 142	145 / 136	90 / 84	91 / 106	132 / 133	17 / 133	127 / 128	118 / 131
SILK	131 / 142	130 / 122	149 / 151	153 / 151	139 / 117	66 / 127	61 / 119	49 / 72	88 / 73
SegOF	132 / 147	62 / 127	74 / 84	143 / 144	148 / 151	80 / 135	83 / 124	114 / 146	143 / 136
IAOF2	133 / 98	60 / 121	134 / 138	94 / 75	135 / 79	131 / 132	90 / 121	116 / 76	109 / 63
StereoFlow	134 / 136	149 / 152	112 / 143	87 / 59	69 / 78	107 / 152	143 / 153	78 / 61	138 / 124
H+S_ROB	135 / 148	70 / 112	117 / 118	138 / 153	128 / 126	63 / 136	107 / 102	132 / 144	133 / 135
PGAM+LK	136 / 143	142 / 146	144 / 137	140 / 143	151 / 147	92 / 123	45 / 115	29 / 94	124 / 121
FGIK	137 / 8	148 / 7	108 / 26	106 / 57	96 / 57	58 / 13	53 / 7	146 / 2	154 / 6
Rannacher	138 / 125	68 / 104	140 / 132	142 / 132	61 / 77	98 / 102	79 / 88	149 / 130	114 / 128
ContinualFlow_ROB	139 / 130	54 / 137	46 / 87	131 / 89	144 / 141	140 / 149	94 / 75	138 / 122	147 / 143
Shiralkar	140 / 135	120 / 132	118 / 121	130 / 120	129 / 142	84 / 137	80 / 85	139 / 140	139 / 146
IIOF-NLDP	141 / 140	113 / 109	91 / 101	117 / 110	109 / 110	88 / 126	147 / 143	154 / 152	131 / 134
TV-L1-improved	142 / 116	138 / 43	138 / 129	110 / 126	111 / 16	122 / 98	99 / 96	134 / 133	112 / 89
StereoOF-V1MT	143 / 129	128 / 130	133 / 103	144 / 130	125 / 136	117 / 103	103 / 112	111 / 138	81 / 70
2bit-BM-tele	144 / 137	139 / 119	122 / 123	86 / 133	87 / 84	147 / 72	150 / 146	150 / 153	33 / 36
IAOF	145 / 106	147 / 123	147 / 152	151 / 123	118 / 109	101 / 74	85 / 68	141 / 80	63 / 37
Pyramid LK	146 / 153	127 / 145	141 / 153	123 / 152	153 / 154	78 / 153	74 / 93	129 / 147	155 / 154
Adaptive flow	147 / 110	146 / 110	151 / 144	98 / 64	149 / 115	142 / 144	145 / 140	56 / 39	135 / 78
SimpleFlow	148 / 145	74 / 52	105 / 98	152 / 148	84 / 41	148 / 128	148 / 142	151 / 149	137 / 144
Heeger++	149 / 144	153 / 148	113 / 135	128 / 140	108 / 134	149 / 148	117 / 108	113 / 145	152 / 141
SPSA-learn	150 / 150	133 / 141	132 / 112	145 / 145	121 / 128	112 / 114	141 / 62	137 / 151	148 / 152
WOLF_ROB	151 / 146	155 / 153	137 / 145	136 / 131	140 / 140	141 / 145	66 / 145	133 / 148	142 / 147
WRT	152 / 152	111 / 118	131 / 113	147 / 147	101 / 114	124 / 142	151 / 150	144 / 154	151 / 153
GroupFlow	153 / 151	150 / 151	128 / 124	155 / 142	150 / 150	133 / 151	104 / 151	140 / 141	149 / 148
AVG_FLOW_ROB	154 / 155	144 / 155	152 / 155	127 / 155	154 / 155	154 / 155	155 / 155	155 / 155	132 / 155
Periodicity	155 / 154	154 / 154	154 / 154	150 / 150	155 / 153	153 / 154	154 / 154	152 / 150	153 / 150